Progress in Polymer Science 66 (2017) 1–21

Contents lists available at ScienceDirect

Progress in Polymer Science

journal homepage: www.elsevier.com/locate/ppolysci

Scattering perspectives on nanostructural inhomogeneity in polymer network gels

Sebastian Seiffert

Institute of Physical Chemistry, Johannes Gutenberg-Universität Mainz, Duesbergweg 10–14, D-55128 Mainz, Germany

ARTICLE INFO

Article history:
Available online 28 December 2016

Keywords:
Crosslinking
Gel
Inhomogeneity
Polymer network
Scattering

ABSTRACT

Scattering methods based on spatial and temporal contrast fluctuations in polymer-network gels, which originate from polymer-segmental density fluctuations, reveal rich insight into different types and levels of nanostructural inhomogeneity in these soft materials. Complementary contrasting as provided by light, neutron, and X-ray scattering allows such information to be obtained on nano- to micrometer length scales. On top of that, complementary use of static and dynamic scattering methods allows the interplay and effect of these inhomogeneities to be unraveled. This article interrelates a multitude of studies on the application of scattering techniques for analytical assessment of structural inhomogeneity in polymer-network gels conducted since the 1970s.

Contents

1. Introduction

Polymer-network gels consist of three-dimensionally crosslinked chain molecules swollen with a solvent [1]. They can be formed by different methods, most typically based on uncontrolled chain-growth polymerization abetted by in-situ crosslinking, as shown in Fig. 1a, or on better controlled random or regular interconnection of pre-polymerized building blocks, as shown in Fig. 1b and c. Depending on the conditions during these different ways of formation, and depending on the conditions during the subsequent state of observation, polymer-network gels exhibit diverse and complex nanoscopic architectures [2,3]. Commonly, the polymer-network mesh topology on scales of 1–10 nm is not uniform and regular, as idealized in Fig. 1c, but polydisperse and irregular, as sketched in Fig. 1b. On top of that, many swollen polymer networks display a further level of spatial inhomogeneity on scales of 10–100 nm and beyond, as sketched in Fig. 1a. This structural complexity markedly affects the optical clarity, mechanical strength, and permeability of polymer gels, which is of central relevance for their performance in popular applications such as those as superabsorbers [4], soft contact lenses [5,6], carriers of bioactive agents [7,8], and matrixes in the analytical sciences [9–13]. As a result, polymer-network inhomogeneity has been a vibrant field of research since the 1970s [14]. This article reviews a core part of this extensive research, with a focus on the analytical assessment of structural inhomogeneity in polymer-network gels by scattering techniques. Such work experienced increasing popularity since its first remarkable notion four decades ago and then climaxed in the early 2000s, as

E-mail address: sebastian.seiffert@uni-mainz.de

http://dx.doi.org/10.1016/j.progpolymsci.2016.12.011
0079-6700/

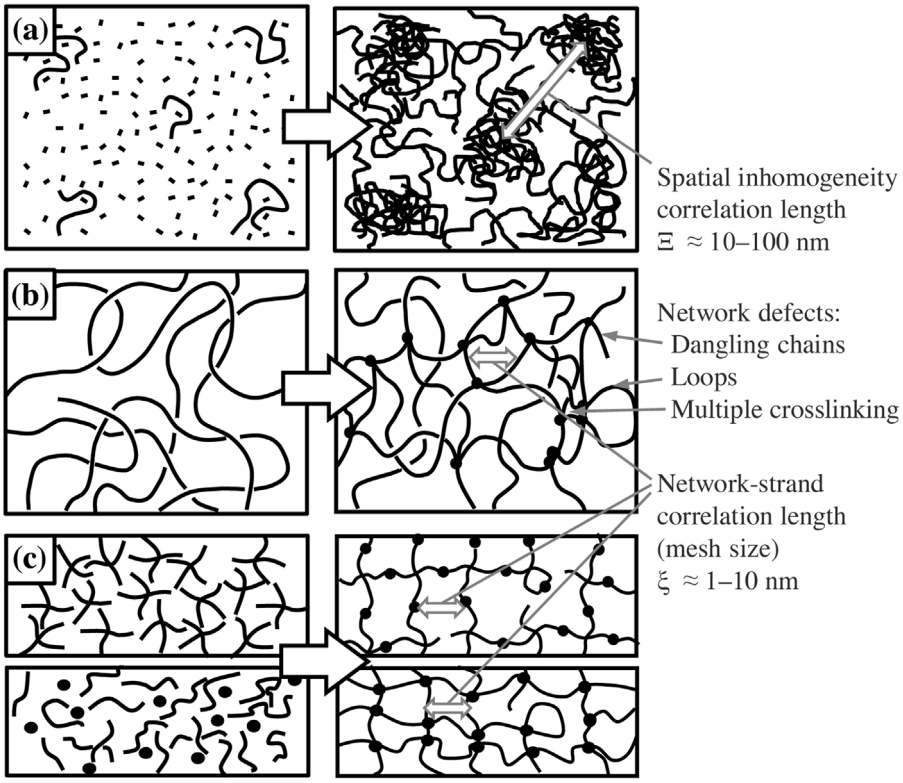

Fig. 1. Polymer-network architectures as obtained by three different approaches of gelation, each illustrated in one of the figure panels. (a) Formation of an irregular and spatially inhomogeneous polymer-network gel by uncontrolled chain-growth crosslinking copolymerization of monomers and crosslinkers, thereby causing static spatial variation of the polymer-segmental and crosslinking density on scales of 10–100 nm. (b) Formation of a just locally inhomogeneous polymer-network gel by random crosslinking of side-functionalized chains in a semidilute solution, thereby forming polydisperse network meshes on scales of 1–10 nm but no additional spatial inhomogeneity on larger scales as those illustrated in panel a. (c) Formation of a potentially regular and homogeneous polymer-network gel by cross-coupling of complementarily functionalized star-polymer building blocks (upper half-panel) or end-linking of suitably capped chains to functional linkers (lower half-panel). [2,3], Copyright 2014 and 2015. Adopted with permission from Wiley-VCH.

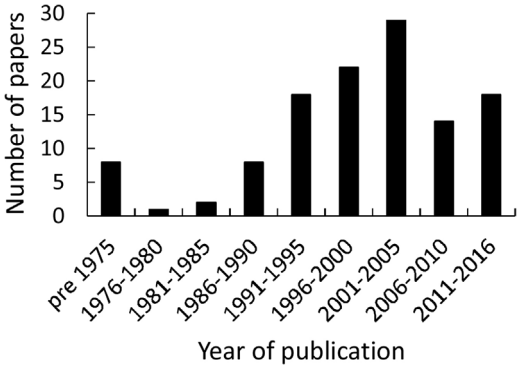

Fig. 2. Publication record of the original research papers reviewed in this article (excluding references to other review articles or books).

visualized in Fig. 2, when research on polymer networks and gels attracted remarkable fundamental interest. In the following half decade, the publication activity first decreased, but since about 2010, there is re-growing interest, as also seen in Fig. 2. This is due to two developments. First, the field has witnessed seminal breakthroughs in the attempt of preparing defect-free model-type polymer networks based on controlled polymerization and on click chemistry; these model networks both serve as a material basis to (re-)address a plethora of fundamental polymer-physical questions, and as a class of highly tough and resilient gels. Second, in quite a contrast to these model-network gels, there is increasing interest in multi-scale hierarchical structural complexity in soft matter, including inhomogeneous and porous gels, which have promise to serve as membranes in energy conversion devices and in laboratory analytics. This article aims to bridge these early insight-oriented and recent application-oriented developments in view of consistently and comprehensively cross-relating the existing picture of polymer-network structural inhomogeneity as gained by scattering methods.

2. Norms and nomenclature

Polymer-network inhomogeneity in a gel manifests itself in various forms spanning multiple length scales, as indicated in Fig. 1. To account for this diversity, several schemes of classification have been introduced.

Norisuye, Shibayama, and co-authors differentiated between two types of inhomogeneities in polymer-network gels. One is imparted during the gelation process by the “freezing-in” of thermal concentration fluctuations at the gelpoint, which are particularly strong if the gelling system is close to its phase-boundary spinodal line [15–17]. The static polymer-network inhomogeneity resulting from this process has been referred to as “frozen concentration fluctuation” [15,17–23], “frozen blobs” [24], “frozen inhomogeneity” [16,25], and “frozen elastic constraints” [26], and it is a central motif in a closely related theory on gel polymer-network structures introduced by Panyukov and Rabin [27–30]. On top of these frozen concentration fluctuations, a further type of inhomogeneity manifests itself in the form of a non-random irregular distribution of the crosslinking junctions in a gel, as sketched in Fig. 1a, which was detected in light-scattering studies by Norisuye, Shibayama, and co-workers [17].

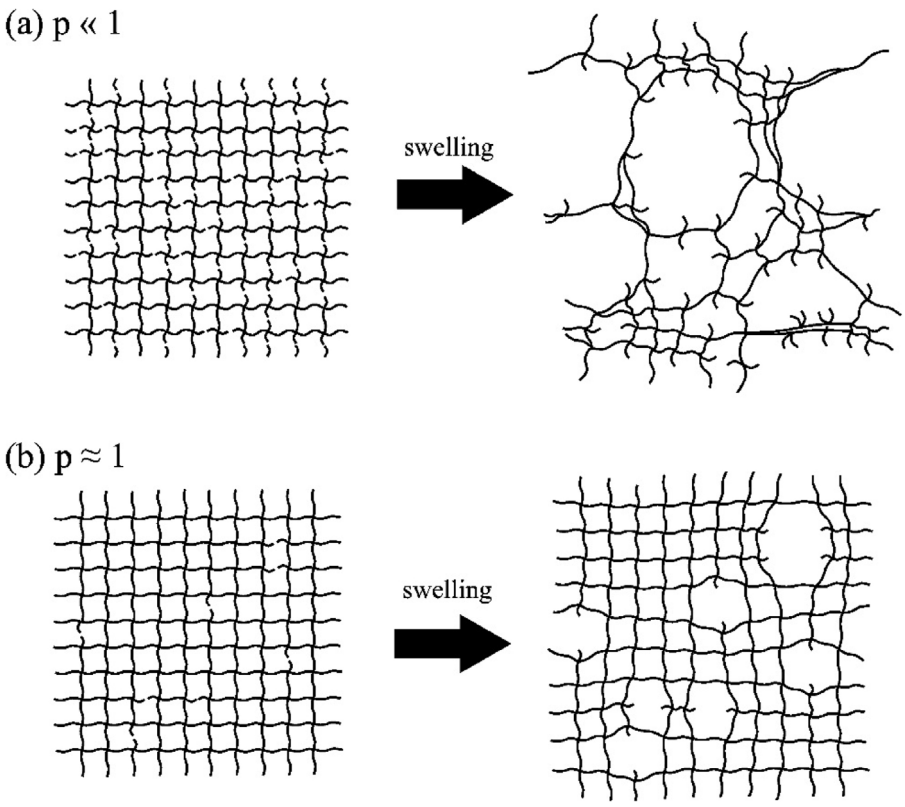

Fig. 3. Interrelation of local network defects and spatial concentration inhomogeneities in polymer-network gels in the cases of strong (panel a) and weak (panel b) network imperfection, as distinguished from one another by Grube and Oppermann [34] and further unraveled by Shibayama, Sakai, and co-workers [41]. In the latter study, gels were made by polymer-analogous crosslinking of monodisperse regular and uniform star-polymer building blocks, as sketched in Fig. 1c (upper half-panel), conducted such to compare gels with different controlled extents of local defects at (a) low ($p \ll 1$) or (b) high ($p \approx 1$) degree of coupling of building blocks that have defined fractions of end-functionalization imperfection. The resulting gels show nearly the same weakly inhomogeneous structures in their deswollen states (left-hand schemes), whereas they show strongly differing inhomogeneous structures in their swollen states (right-hand schemes). That means that polymer-network spatial crosslinking inhomogeneity is coupled to the polymer-segmental concentration inhomogeneity, which is detectable by scattering methods, only in swollen gels, but not in deswollen gels. [41], Copyright 2014.

Reproduced with permission from the American Chemical Society.

Alternative to this binary scheme of classification, Norisuye and Shibayama also introduced a different scheme of classification in a concurrent series of publications [31,32] that distinguishes between *three* types of polymer-network inhomogeneities. These are (i) spatial inhomogeneities, referring to non-uniform spatial distribution of the crosslinking junctions, as sketched in Fig. 1a, (ii) topological inhomogeneities, which encompass network defects such as loops, dangling chains, and local multiple crosslinking, as sketched in Fig. 1b, and (iii) connectivity inhomogeneities, related to the size distribution of nano- and microgel clusters at the gelation threshold, relevant only during the process of gel percolation. In a recent publication by Asai, Sakai, Shibayama, and co-authors aiming to unravel interdependences between these three types of inhomogeneities, the latter two were both regarded as "local inhomogeneities" and denoted to be a potential origin of the first, regarded as "spatial inhomogeneity", provided that the local inhomogeneities are present to a marked extent during the process of gelation [33].

In contrast to the latter indication of interdependence of local and spatial inhomogeneities, Grube and Oppermann pointed out the necessity to sharply *distinguish* between "concentration" and "network density" (=connectivity + topological) inhomogeneities [34], which is a scheme of classification closely corresponding to that by Shibayama, Norisuye, and colleagues [17]. In earlier literature, these two types of inhomogeneities were often assumed [35–40] or lately demonstrated [33] to be apparently or actually coupled to one another. However, as Grube and Oppermann have shown, there is no such coupling in a state of gel preparation, where network-defect inhomogeneity depends on the concentration and reactivity of the active species in the gelling system, whereas the extent of concentration inhomogeneity depends on the extent of diffusive mass redistribution in it. Post-gelation swelling, however, generally entails strong concentration inhomogeneity, as it translates network-defect inhomogeneity into spatial concentration fluctuation. A conceptually similar finding has been reported by Shibayama, Sakai, and co-authors on defect-controlled tetraPEG gels, as shown in Fig. 3 [41].

In yet another scheme of classification, Okay delimited the term "inhomogeneity", referring to "*fluctuation of the crosslink density in space*" from the term "heterogeneity", referring to "*the existence of phase-separated domains in polymer gels*" [42]. This view is in line with an earlier perspective by Dušek and Prins, who denoted "heterogeneous" gels to be formed by microsyneresis during their gelation [14]. With that, another level of polymer-network structural complexity is regarded, encompassing sponge-like gels penetrated by nano- to millimeter-sized pores [43].

3. Scattering by polymer-network inhomogeneity

Scattering of radiation or quantum objects is caused by density fluctuations on length scales assessed by the scattering wave vector, $\mathbf{q} = \mathbf{k}_i - \mathbf{k}_s$, where $\mathbf{k}_i$ and $\mathbf{k}_s$ are the wave vectors of the incident and the scattered radiation. In the limit of elastic scattering, $k_i = k_s = 2\pi/\lambda$, such that $q = (4\pi/\lambda) \sin(\theta/2)$, with λ the

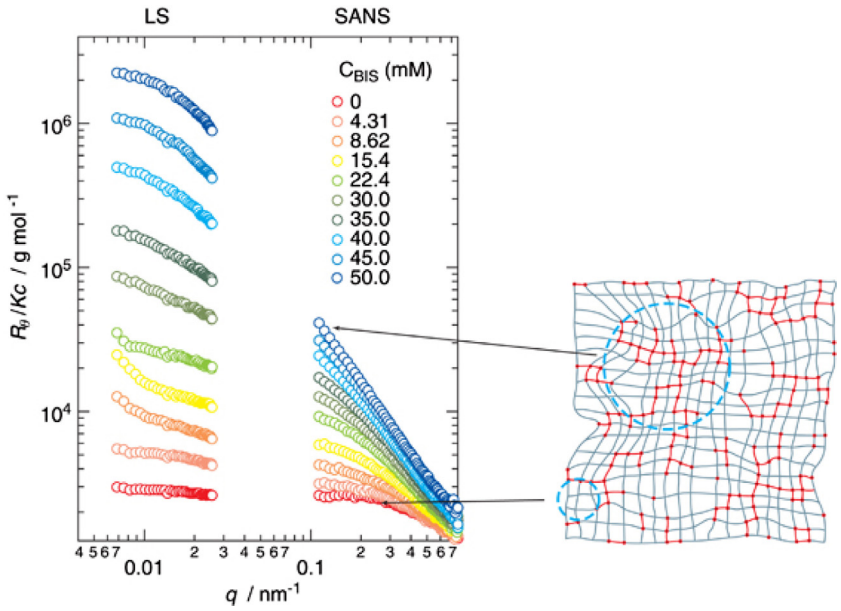

Fig. 4. Small-angle neutron scattering (SANS) and light scattering (LS) data of swollen poly(*N*-isopropylacrylamide) hydrogels prepared with different concentrations of crosslinker, *N*,*N*′-methylenebisacrylamide (BIS), along with a schematic representation of the inhomogeneous gel structure that displays multiple levels of structural correlations on different lengthscales. These different structural features are reflected at different ranges of the scattering wave vector q: whereas local correlations of the polymer-network mesh structure are reflected at high q, spatial crosslinking inhomogeneity is reflected at low q. To cover all of these ranges, complementary use of SANS and LS is mutually supportive. Note that a similar graph has been published by Hecht, Duplessix, and Geissler [44]. The scheme on the right was originally introduced in [24]; copyright 1988 ACS. [48], Copyright 2011.

Reproduced with permission from the Nature Publishing Group.

radiation wavelength in the medium and θ the scattering detection angle. In polymer-network gels, scattering is most relevantly caused by fluctuations on scales of 1–100 nm; this largely corresponds to the realm of *spatial inhomogeneity* according to the above schemes of classification. In the words of Okay: "*since gel inhomogeneity is closely connected to the spatial concentration fluctuations, scattering methods* [. . .] *have been employed to investigate the spatial inhomogeneities*" [35–40]. It is commonly assumed and practically turns out to work well [44], and it has also been consistently proven [26] that polymer-network concentration fluctuations on these length scales similarly cause light, X-ray, and neutron scattering. According to the above formula, the range of q^{-1} = 1–100 nm is covered when scattered X-rays or neutrons with wavelengths of λ = 0.02–0.5 nm are detected at angles well below 1°, commonly referred to as small-angle scattering, whereas scattering of light (λ = 400–700 nm) is best observed at angles of 30–150° to cover and extend this range. On this common ground, data obtained by these different methods can be superimposed to becoming master curves that span a large range of the scattering wave vector, as shown in Fig. 4. With that, length scales of 0.5–500 nm are covered [23,44–48], comprising multiple structural features of polymer-network gels that range from their local polymer-segmental correlations and network mesh sizes on scales of ξ = 1–10 nm (high q, neutron and X-ray scattering regime), as illustrated in Fig. 1b and c, to spatial inhomogeneities on scales of Ξ = 10–100 nm and beyond (low q, light scattering regime), as illustrated in Fig. 1a.

When polymer-network gels are probed on such large ranges of q, notable excess forward scattering is observed. This observation has actually first been reported for some uncrosslinked semidilute and concentrated polymer solutions [49,50], but the effect is even stronger in crosslinked gels and gets more pronounced at stronger crosslinking [51,52]. In a pioneering systematic study, Geissler, Horkay, Hecht, and co-workers have quantitatively assessed this low-q scattering by use of complementary small-angle X-ray and neutron scattering (SAXS and SANS), both calibrated to absolute units [26]. The scattering curves of end-linked poly(dimethylsiloxane) (pDMS) network-gels in organic media obtained by these two independent methods coincide, revealing the excess scattering not to stem from chemical inhomogeneity, but from topological inhomogeneity in the gels. The same researchers have also shown that SANS [51] and SAXS [53] data obtained from poly(vinyl alcohol)-based homo- [51] and copolymer [53] gels can be fitted to a sum of a Lorentzian and a stretched-exponential term, denoted to separately account for dynamic and static scattering contributions. The identity of these two scattering contributions was proven by independent dynamic light scattering (DLS) measurements, which coincide with the dynamic parts isolated from the SANS or SAXS data sum-fitting; the same finding was also made for end-linked polyfluorosilicone (PFS) organogels by mutually supportive DLS and neutron spin echo (NSE) experiments [54]. Based on this independent additivity, it was further shown that only the static parts display considerable variation with the polymer-network crosslinking density, which manifests itself in the form of an increasing correlation length of the polymer concentration in the gel, denoting the gel structure to be "*redistributed into more and less densely crosslinked local domains*" [51]. By contrast, in other work, the dynamic correlation length associated to network-strand fluctuation in dynamic light scattering experiments was found to decrease with increasing crosslinking density, denoting the network mesh size to decrease upon crosslinking [55].

In another fundamental study, Koizumi and colleagues used small-angle neutron scattering (SANS) in conjunction with neutron spin echo (NSE) to decompose the neutron scattering data into static and thermal contributions [21,56]. This decomposition proves that the static parts contribute a squared-Lorentzian scattering profile that has a steep $I \sim q^{-4}$ tail at high q, whereas the thermal parts contribute a simple Lorentzian that dominates in this region due to its shallower $I \sim q^{-2}$, as shown in Fig. 5a. On top of that lies an additional squared-Lorentzian that contributes dominant additional $I \sim q^{-4}$ scattering at low q [54], as also shown in

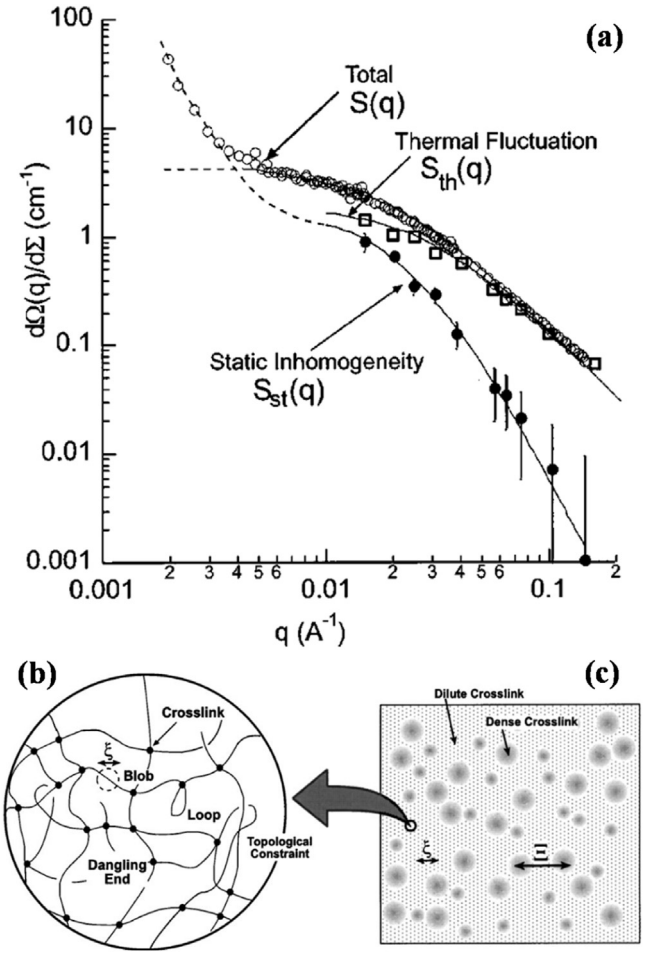

Fig. 5. (a) Small-angle neutron scattering (SANS, open circles) and neutron spin echo (NSE, filled circles and open squares) data obtained of poly(*N*-isopropylacrylamide) hydrogels, along with (b, c) schematics of the gel structures addressed to be reflected in the scattering data. The solid lines in panel a represent calculations by the Panyukov–Rabin theory, predicting a simple Lorentzian and a squared Lorentzian function for the thermal and the static scattering components of the 'frozen' blob structure on scales of single to several ξ, respectively. These functions display asymptotic tails of q^{-2} and q^{-4} at high q, the first of which dominating in this region. On top of that, at low q, lies an additional squared-Lorentzian that gives raise to dominant low-q upturn of the scattering intensity. This additional contribution reflects further polymer-network crosslinking- and segmental-density inhomogeneities on a larger scale of Ξ. (b, c) Schematic of the gel structure on scales of (b) about twenty nanometers and (c) about hundred nanometers. [56], Copyright 2004.

Reproduced with permission from AIP.

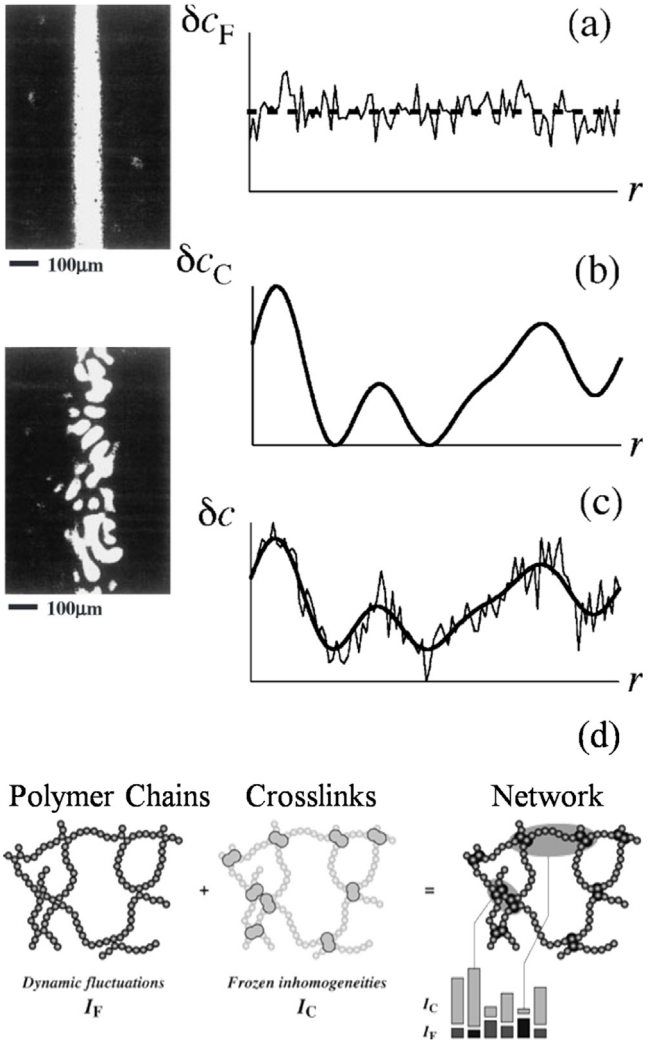

Fig. 6. Two kinds of concentration fluctuations in a polymer-network gel: (a) thermal fluctuations, (b) frozen inhomogeneities, (c) superposition of the two. The left-side micrographs show traces of laser light beams passing through (a) a suspension of polystyrene latex particles and (b,c) a polymer gel. (d) Different extent of the thermal and static contributions in different locations of a gel: in general, densely crosslinked local domains are characterized by strong static and weak dynamic concentration fluctuations, whereas loosely crosslinked domains are characterized by weak static and strong dynamic concentration fluctuations. [57] and [60], Copyright 2004 and 2006, respectively.

Reproduced with permission from the American Chemical Society and the Chemical Society of Japan, respectively.

Fig. 5a. The simple Lorentzian contribution reflects dynamic segmental fluctuations that occur on the blob length scale ξ, similar to those in a semidilute polymer solution of the same concentration, as illustrated in Fig. 5b. By contrast, the two squared-Lorentzian contributions reflect static "frozen" concentration fluctuations on scales of the "frozen blobs" [54], corresponding to several ξ, as well as a on scales of larger polymer-network crosslinking- and segmental-density inhomogeneities, Ξ, as illustrated in Fig. 5c.

On the basis of these fundamental studies, the three methods of light, small-angle X-ray, and small-angle neutron scattering (LS, SAXS, and SANS) were proven to be suitable to quantitatively assess polymer-network inhomogeneity on multiple length scales in a decoupling fashion. To make this truly useful, these methods are often combined with one another, and this effort is often further supported by additional swelling or mechanical measurements.

3.1. Light scattering

Light scattering is based on fluctuations of the refractive index on scales comparable to that of the light wavelength. These fluctuations are inherently connected to density or concentration fluctuations in the sample. In a polymer-network gel, there are two sorts of such concentration fluctuations: static, time-constant spatial variation of the polymer concentration, δc_C, and dynamic concentration fluctuations, δc_F, as schematized in Fig. 6a–c. The time-constant spatial variation of the polymer concentration causes a notable speckle pattern of the light scattering intensity on scales of several ten micrometers, as also shown in Fig. 6 [57]; this is often addressed as a simple qualitative measure of the gel inhomogeneity [20,55,57,58]. On top of that, the dynamic fluctuations superimpose additional time-dependent variation of the scattering intensity around its local average, as illustrated in Fig. 6d. Based on

that, two variant methods of light scattering are available: static light scattering (SLS) [59] and dynamic light scattering (DLS) [60].

3.1.1. Static light scattering

Static light scattering (SLS) probes the time-averaged scattering intensity as a function of the scattering angle, expressed in terms of the magnitude of the scattering wave vector, $q = (4\pi/\lambda)\sin(\theta/2)$. Evaluation of these data is performed on the basis of different conceptual models to draw conclusions about the nanostructural features that cause the light scattering as measured.

The scattering intensity of a gel, which is commonly quantified by its Rayleigh ratio [61], $R_{gel}(q)$, is generally larger than that of a comparable semidilute solution of the same polymer at the same concentration, $R_{sol}(q)$ [35–40]. This is particularly true at low q, whereas the scattering of polymer gels and solutions is more alike at high q [62], as seen in Fig. 4. A cause of this effect is that the q-dependence of the gel-scattering is stronger than that of the scattering by solutions, displaying a stronger upturn at low q, as also seen in Fig. 4. These effects are because the scattering of a solution is due to thermal concentration fluctuations alone, which are most relevant at high q, associated to length scales of $\xi = 1$–10 nm (Fig. 5b), whereas that of a gel has an extra contribution due to permanent static concentration fluctuations, $R_{ex}(q)$, that are particularly strong at low q, associated to length scales of $\Xi = 10$–100 nm (Fig. 5c). It has been demonstrated by several studies that these two contributions are additive and independent of one another in polymer gels, as visualized in Fig. 6. For example, Joosten, McCarthy, and Pusey have shown that upon increasing the gel-network crosslinking density at a constant polymer concentration, the static part of the scattering intensity increases considerably, whereas the dynamic part is barely affected and has a magnitude similar to that in an uncrosslinked solution [62]. The same finding has also been reported by Shibayama, Norisuye, and co-workers [55,60], by Horkay, Hecht, and Geissler [51], and by Krahl, Boyko, and Arndt [63]. This observation indicates that the dynamic fluctuations are the same in a solution and in a gel, whereas the static contribution is added on top of them in a gel, as seen in Figs. 4 and 5 and schematized in Fig. 6; this is much further pronounced by swelling, as illustrated in Fig. 3 [25,63]. In another work, Shibayama, Takata, and Norisuye have shown that dynamic fluctuations in temperature-sensitive gels depend neither on the crosslinking density nor on the preparation temperature, whereas the static fluctuations do; this observation further indicates the dynamic fluctuations to be the same as in a solution, depending only on the experimental conditions at the moment of observation, whereas the static fluctuations are permanently imparted into the gel at the moment of its formation and therefore depend on the experimental conditions at this instant [17,19]. As a result, the latter can be determined from the simple difference $R_{gel}(q) - R_{sol}(q) = R_{ex}(q)$.

According to Debye and Bueche [64,65], and related to work by Pekeris [66], the excess scattering intensity that arises from the time-constant spatial crosslinking inhomogeneity in a polymer gel is

$$R_{ex}(q) = \frac{4\pi K \Xi^3 \langle \eta^2 \rangle}{\left(1 + q^2 \Xi^2\right)^2} \tag{1}$$

if the spatial correlation function of the time-constant refractive-index variation obeys a simple exponential decay, $\exp(-r/\Xi)$, [61], as it does in polymer gels and many other media. In this equation, $K = 8\pi^2 n^2 \lambda^{-4}$ with n the refractive index of the medium and λ the wavelength of the incident and scattered light. A central parameter is $\langle \eta^2 \rangle$, which is the mean-square fluctuation of the refractive index in the sample caused by its static concentration fluctuation that spreads on a correlation length scale Ξ. Linearization of this equation in the form of

$$R_{ex}(q)^{-1/2} = \left(2\sqrt{\pi K \Xi^3 \langle \eta^2 \rangle}\right)^{-1} + \tfrac{1}{2}\sqrt{\frac{\Xi}{\pi K \langle \eta^2 \rangle}} \cdot q^2 = b + m \cdot q^2 \tag{2}$$

allows the latter parameters to be derived from the slope, m, and intercept, b, of a plot of $R_{ex}(q)^{-1/2}$ vs. q^2 [61], yielding $\Xi = (m/b)^{0.5}$ and $\langle \eta^2 \rangle = (4\pi K m^{1.5} b^{0.5})^{-1}$ [35]. With this approach of data analysis, several light scattering studies conducted on various polymer-network gels have been evaluated in view of determining the parameters $\langle \eta^2 \rangle$ and Ξ to quantitatively express the gel polymer-network inhomogeneity and to study it as a function of different experimental parameters that impact the gel preparation, most prominently the monomer and crosslinker concentrations [35,36,38,67–72] and reactivities [37,40,73,74], the gel preparation temperature [72], and rate of the gelation reaction [39]. In such assessment, additional expressiveness can be achieved by translation of the mean-square variation of the refractive index, $\langle \eta^2 \rangle$, into a mean-square variation of the concentration, $\langle c^2 \rangle$, by use of the refractive index increment, which allows the relative concentration fluctuation on the length scale ξ to be quantified as $\langle c^2 \rangle^{1/2}/c$ [72].

Related to the Debye–Bueche approach, alternative expressions for the excess scattering intensity caused by the static crosslinking inhomogeneity in a gel are given as either a Guinier-type function [75,76]

$$R_{ex}(q) = 4\pi K \Xi^3 \langle \eta^2 \rangle \cdot \exp\left(-\Xi^2 q^2\right) \tag{3}$$

or an Ornstein–Zernike-type function [77]

$$R_{ex}(q) = \frac{4\pi K \Xi^3 \langle \eta^2 \rangle}{1 + q^2 \Xi^2} \tag{4}$$

These functions can be linearized in plots of $\ln[R_{ex}(q)]$ vs. q^2 (Guinier plot) or $R_{ex}(q)^{-1}$ vs. q^2 (Ornstein–Zernike plot) to determine $\langle \eta^2 \rangle$ and Ξ as $\Xi = |m|^{0.5}$ and $\langle \eta^2 \rangle = \exp(b) \cdot (4\pi K |m|^{1.5})^{-1}$ (Guinier plot) or $\Xi = (m/b)^{0.5}$ and $\langle \eta^2 \rangle = b^{0.5}(4\pi K m^{1.5})^{-1}$ (Ornstein–Zernike plot). These methods of data analysis are usually applicable just as well as the Debye–Bueche approach [35].

Several decades after development of the Debye–Bueche method, Panyukov and Rabin [27,28] used replica field theory methods to model the network structure of randomly crosslinked polymer gels formed by random instantaneous crosslinking of linear chains in a good solvent at semidilute concentration. This concept is based on the separation of solid-like and liquid-like degrees of freedom [29] to model the density correlation function, and hence, the structure factor of polymer gels:

$$S(q) = G(q) + C(q) \tag{5}$$

In this formula, $G(q)$ is a dynamic correlator that accounts for thermal density fluctuations in the gel, whereas $C(q)$ is a static correlator that accounts for its static inhomogeneity. These contributors are predicted [28] to be

$$G(q) = \frac{\phi N g(q)}{1 + w g(q)} \tag{6}$$

and

$$C(q) = \frac{\phi N}{(1 + w g(q))^2 \left(1 + Q^2\right)^2} \cdot \left(6 + \frac{9}{w_0 - 1 + 0.5\left(Q_{para}{}^2 \lambda^2 + Q_{perp}{}^2 \lambda^{-1}\right)^2 \left(\phi_0/\phi\right)^{5/12}}\right) \tag{7}$$

In these equations, N is the number of segments between the crosslinking junctions, ϕ and ϕ_0 are the polymer volume fractions at the states of measurement and gel preparation, respectively, and Q is a dimensionless wave vector composed of a parallel and a perpendicular component with $Q^2 = Q_{para}{}^2 + Q_{perp}{}^2$, given as either $Q = I_{Segment} N^{1/2} q$ [28,36,72] or $Q = (1/6)^{1/2} I_{Segment} N^{1/2} q$ [16] in the literature. In Eq. (7), λ denotes the linear swelling ratio, which is given as $\lambda = (\phi_0/\phi)^{1/3}$ in the mean-field limit or slightly modified as $\lambda = (\phi_0/\phi)^{1/3}\phi_0{}^{-1/8}$ in the scaling limit [16]. Several variants of Eq. (7) have been named and used in follow-up publications:

$$C(q) = \frac{\phi N}{(1 + wg(q))^2 \left(1 + Q^2\right)^2} \cdot \left(6 + \frac{9}{w_0 - 1 + 0.5Q^2 \left(\phi_0/\phi\right)^{5/12}} \right) \tag{7a}$$

[72]

$$C(q) = \frac{\phi N}{(1 + wg(q))^2 \left(1 + Q^2\right)^2} \cdot \left(6 + \frac{9}{w_0 - 1 + 0.5Q^2 \left(\phi_0/\phi\right)^{2/3} \phi_0{}^{-1/4}} \right) \tag{7b}$$

[36]

$$C(q) = \frac{\phi N}{(1 + wg(q))^2 \left(1 + Q^2\right)^2} \cdot \left(6 + \frac{9}{w_0 - 1 + 0.5Q^2 \left(\phi_0/\phi\right)^{2/3}} \right) \tag{7c}$$

[17]

$$C(q) = \frac{\phi N}{(1 + wg(q))^2 \left(1 + Q^2\right)^2} \cdot \left(6 + \frac{9}{w_0 - 1 + \left(1/12\right) Q^2 \frac{\phi_0}{\phi}} \right) \tag{7d}$$

[16]

The dimensionless function $g(q)$ was originally [28] given as

$$g(q) = \frac{1}{0.5Q^2 + \left(4Q^2\right)^{-1} + 1} + \frac{2Q^2 \left(\phi/\phi_0\right)^{5/12}}{\left(1 + Q^2\right)^2 \left(Q_{para}{}^2 \lambda^2 + Q_{perp}{}^2 \lambda^{-1}\right)} \tag{8}$$

Again, several different variant forms of it have been published henceforth:

$$g(q) = \frac{1}{0.5Q^2 + \left(4Q^2\right)^{-1} + 1} + \frac{2Q^2 \left(\phi/\phi_0\right)^{12/5}}{\left(1 + Q^2\right)^2 \left(Q_{para}{}^2 \lambda^2 + Q_{perp}{}^2 \lambda^{-2}\right)} \tag{8a}$$

[20]

$$g(q) = \frac{1}{0.5Q^2 + \left(4Q^2\right)^{-1} + 1} + \frac{2\left(\phi/\phi_0\right)^{2/3} \phi_0{}^{1/4}}{\left(1 + Q^2\right)^2} \tag{8b}$$

[36,72]

$$g(q) = \frac{1}{0.5Q^2 + \left(4Q^2\right)^{-1} + 1} + \frac{2\left(\phi/\phi_0\right)^{2/3}}{\left(1 + Q^2\right)^2} \tag{8c}$$

[16,17]

The dimensionsless parameters w and w_0 are the effective virial coefficients in the state of measurement and preparation, respectively. In a mean-field approach, $w = (1-2\chi+\phi)\phi N$ and $w_0 = (1-2\chi_0+\phi_0)\phi_0 N$, with χ the Flory–Huggins polymer–solvent interaction parameter [16,17,36], which turns into $w = \phi^{5/4} N$ and $w_0 = \phi_0{}^{5/4} N$ in the scaling limit at good solvent conditions [17,72], to which the original report [28] was limited [72]. With this set of formulae, the scattering intensity, $I(q)$, can be calculated:

$$I(q) = \frac{N_A}{v_{Segment}} \left[b_{Solvent} \left(\frac{v_{Segment}}{v_{Solvent}} \right) - b_{Segment} \right]^2 S(q) \tag{9}$$

with N_A the Avogadro number, and b_i and v_i the scattering lengths and molar volumes of the segments and the solvent [16]. As an alternative, the Rayleigh ratio, $R(q)$, can be calculated in a similar fashion:

$$R(q) = b^2 I_{Segment}^{-3} S(q) \tag{10}$$

with b the scattering length of the monomeric segments, given by $b = [(2\pi n M_{Segment})/(N_A \lambda^2)] \cdot (dn/dc)$ with c in units of mass per volume and $M_{Segment}$ in units of mass per mole, while $l_{Segment}$ is the statistical segment length [72]. That way, theoretical scattering curves have been calculated for various polymer-network systems, and at least semi-quantitative [32,69,72,78–82] or partially quantitative [16,17] agreement has been found. Deviations have been argued to be because the samples actually studied had different constitutions and formation histories than what is conceptualized in the Panyukov–Rabin model, which relies upon the picture of networks formed by random crosslinking of pre-polymerized chains in a good solvent [72].

To conclude this sub-section, it shall be remarked that the above set of formulae may appear diverse and rather phenomenological, which is not untrue indeed. In this context, the title of this article is twofold: perspectives on gel structures can be gained by scattering, but there is manifold variants of how exactly (that is, with which fitting equation or data analysis procedure) this may to be done, meaning that there's multiple "scattered perspectives" on this. Out of the preceding set of approaches and equations, the Panyukov–Rabin concept may be regarded particularly meaningful, because it received convincing multifaceted experimental support, as discussed in greater detail in Section 4 of this article.

3.1.2. Dynamic light scattering

Whereas static light scattering (SLS) is based upon probing just time-averaged scattering intensities, dynamic light scattering (DLS) focuses on temporal fluctuation of the scattering that occurs as a consequence of dynamic fluctuations of the refractive index in the sample. Through the use of an autocorrelation analysis and with knowledge of the experimental length scale, which is given by the light wavelength and detection angle, these time-resolved intensity fluctuations can be analyzed in view of assessing the dynamics that cause them. A general relation between the time- and angular + wavelength-dependent scattered light intensity, $I(q,t)$, to the amplitude of the electric field scattered into the direction of $\mathbf{q}$ at the time t, $E(q,t)$, is

$$I(q,t) = |E(q,t)|^2 \tag{11}$$

If the sample is composed of many uncorrelated volume elements, then $E(q,t)$ is a zero-mean complex Gaussian variable if it is sampled over the full ensemble of these volume elements [83]. By contrast, a *single* DLS experiment conducted in just one volume element determines the local time-averaged intensity autocorrelation function (ICF) in the form of

$$g_T{}^{(2)}(q,\tau) = \frac{\langle I(q,0) I(q,\tau) \rangle_T}{\langle I(q,0) \rangle_T{}^2} \tag{12}$$

where τ denotes the correlation time and the operator $<\ldots>_T$ denotes time-averaging. Related to this second-order intensity-correlation function is the first-order field-correlation function in the form of

$$g^{(1)}(q,\tau) = \frac{\langle E(q,0) E*(q,\tau) \rangle}{\langle E(q,0)^2 \rangle} \tag{13}$$

where * denotes the Fourier conjugate.

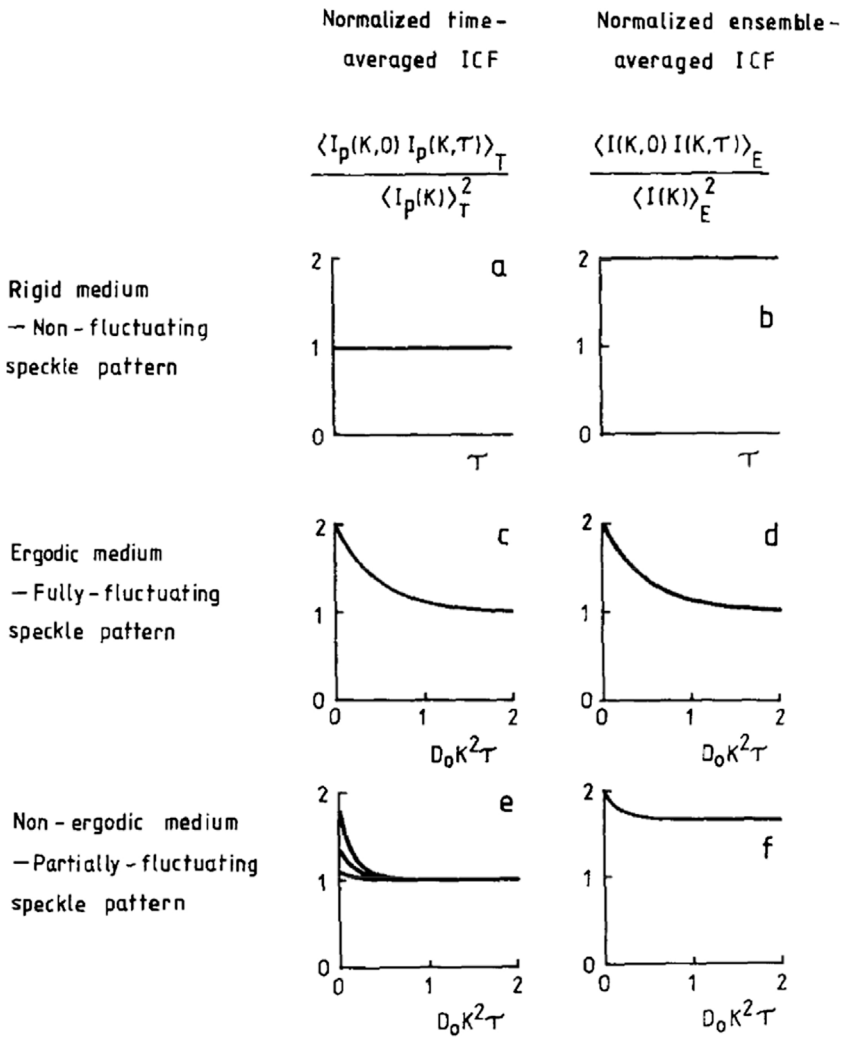

Fig. 7. Normalized time-averaged and ensemble-averaged intensity correlation functions (ICFs) for (a, b) a plain solid medium, (c, d) a plain liquid medium, and (e, f) a gel. [83], Copyright 1989.
Reproduced with permission from Elsevier Ltd.

In a plain solid medium, the intensity recorded in a particular point in the speckle pattern, p, is time-constant, $I_p(q,t) = I_p(q)$, yielding

$$\frac{\langle I_p(q,0)\, I_p(q,\tau)\rangle_T}{\langle I_p(q,0)\rangle_T^{\,2}} = \frac{\langle I_p(q)\, I_p(q)\rangle_T}{\langle I_p(q)\rangle_T^{\,2}} = 1 \tag{14a}$$

whereas sampling over the full ensemble, P, denoted by the operator $<\ldots>_E$, yields

$$\frac{\langle\langle I(q,0)\, I(q,\tau)\rangle_T\rangle_E}{\langle\langle I(q,0)\rangle_T\rangle_E^{\,2}} = \frac{\frac{1}{P}\sum_p I_p^{\,2}(q)}{\left[\frac{1}{P}\sum_p I_p(q)\right]^2} = 2 \tag{14b}$$

due to the zero-mean Gaussian statistical properties of $E(q,t)$. This difference is shown graphically in Fig. 7a and b.

In a plain fluid medium, by contrast, all the different local configurations that persist forever in different local volume elements of a solid are subject to interconvert into one another, and they all occur in just one volume element of a liquid if this is observed on sufficiently long timescales. As a result, the full ensemble can be explored by either sampling over all volume elements at one moment in time or by sampling in just one volume element for a time longer than the correlation time τ. Then

$$\lim_{\tau\to 0} \frac{\langle I(q,0)\, I(q,\tau)\rangle_E}{\langle I(q,0)\rangle_E^{\,2}} = \frac{\langle I^2(q)\rangle_E}{\langle I(q)\rangle_E^{\,2}} = 2 \tag{14c}$$

whereas

$$\lim_{\tau\to\infty} \frac{\langle I(q,0)\, I(q,\tau)\rangle_E}{\langle I(q,0)\rangle_E^{\,2}} = \frac{\langle I(q,0)\rangle_E \langle I(q,\tau)\rangle_E}{\langle I(q)\rangle_E^{\,2}} = 1 \tag{14d}$$

as shown in Fig. 7c and d. The time-averaged ICF, $g_T^{(2)}(q,\tau)$, is then identical to the ensemble-averaged ICF, $g_E^{(2)}(q,\tau)$, and can be related to the normalized field-correlation function or dynamic structure factor (often also referred to as "intermediate correlation function" of the refractive index or density fluctuations [83]), $g^{(1)}(q,\tau)$, via the Siegert relation [84]:

$$g_T^{(2)}(q,\tau) = \frac{\langle I(q,0)\, I(q,\tau)\rangle_T}{\langle I(q,0)\rangle_T^{\,2}} = \frac{\langle I(q,0)\, I(q,\tau)\rangle_E}{\langle I(q,0)\rangle_E^{\,2}} = g_E^{(2)}(q,\tau) = 1 + \beta\left|g^{(1)}(q,\tau)\right|^2 \tag{15}$$

β is the coherence factor of the instrument, which can be estimated from correlation functions recorded on well-defined systems such as dispersions of monodisperse polymer latexes [85]. In

a simple liquid medium like a colloidal-particle suspension, this function decays as a simple exponential, as seen in Fig. 7c and d:

$$g^{(1)}(q,\tau) = \exp\left(-Dq^2\tau\right) \tag{16}$$

with D the translational diffusion coefficient of the scatterers (for example, the colloidal particles), which is related to their hydrodynamic radius, R_h, by the Stokes–Einstein equation:

$$R_h = \frac{kT}{6\pi\eta D} \tag{17}$$

with η the dynamic viscosity of the medium.

The overlay of both dynamic thermal and static "frozen" concentration fluctuations in a polymer-network gel, as schematized in Fig. 6, renders these media to display both fluid-like and solid-like characteristics. Their fluid-like characteristics allow them to display local dynamics, causing exponential decay of local individual time-averaged ICFs, but their co-existing solid-like permanent concentration fluctuations cause this to be different in different scattering volumes in the gel sample, as illustrated in Fig. 6d, thereby creating a speckle pattern with spatial variations of the scattered light intensity on scales of several micrometers, as seen in Fig. 6b. If not taken into account properly, this non-ergodicity may render the analysis of polymer-gel light scattering data prone to impairment [83]. If this complexity is taken into account correctly, however, such scattering data can be consistently decomposed into static and dynamic contributions, thereby yielding information on both the extent of static spatial inhomogeneity and the overlaying thermal dynamics in polymer-network gels. To perform such data analysis, two methods have been introduced.

In one approach, Pusey and van Megen considered the peculiarity of dynamic light scattering on non-ergodic media, with a special focus on polymer gels [83], based on the conceptual approach of harmonically-bound Brownian particles [86] that can undergo diffusive displacement at short times but that find themselves restricted to a maximum displacement at longer times, when the elastic energy equals the thermal energy in the form of $\kappa\langle x\rangle^2 = kT$. Pusey and van Megen stated that the scattering by a polymer-network gel is subject to similar restriction of thermal fluctuations around a mean value, and due to the spatial inhomogeneity of the gel, this mean value varies across the speckle pattern, as shown in Fig. 6c and d. In this case, $E_p(q,t)$ sampled in a single speckle, p, is *not* a zero-mean complex Gaussian variable because its fluctuations are restricted. As a result, the time- and ensemble-averaged scattering intensities are different. At $\tau = 0$, the normalized time-averaged ICF in a single speckle of the scattering pattern, arising from a particular configuration of the sample, has a value less than 2, as shown in Fig. 7e, since only a limited range of intensity fluctuations is sampled there. By contrast, the normalized ensemble-averaged ICF has a value of 2 at $\tau = 0$, as shown in Fig. 7f, because in the full spatial ensemble $E(q,t)$ still is zero-mean complex Gaussian variable. At times longer than τ, the time-averaged ICF from each speckle still decays to 1, as shown in Fig. 7e, since the restricted local fluctuations still become uncorrelated at long times, but different manifestations of this principle form are found in different points in the speckle pattern, as also shown in Fig. 7e. Furthermore, due to the restriction of the fluctuations in each of these speckles, the ensemble-averaged ICF does not decay to 1 at long times, as shown in Fig. 7f. This complex situation renders the Siegert relation [84] invalid and indicates the necessity to sample ICFs at many different speckles in the scattering pattern, corresponding to many different orientations of the sample in the setup, generally more than 100 [87] and in some work up to 2000 [62], to obtain the normalized ensemble-averaged dynamic structure factor, $f(q,\tau)$, analog to $g^{(1)}(q,\tau)$ in an ergodic liquid. To circumvent this tedious necessity, Pusey and van Megen devised a method based on sampling the time-averaged ICF in just *one* single speckle, and hence, operating with just one single sample orientation, and then normalizing it with a factor that contains the spatially averaged mean scattering intensity sampled over the whole specimen:

$$\begin{aligned} g_T^{(2)}(q,\tau) &= \frac{\langle I(q,0)I(q,\tau)\rangle_T}{\langle I(q,0)\rangle_T{}^2} \\ &= 1 + Y^2\left([f(q,\tau)]^2 - [f(q,\infty)]^2\right) \\ &\quad + 2Y(1-Y)([f(q,\tau)] - [f(q,\infty)]) \end{aligned} \tag{18}$$

[83]

or, vice versa,

$$f(q,\tau) = 1 + \frac{1}{Y}\left(\sqrt{g_T^{(2)}(q,\tau) - \sigma_I{}^2} - 1\right) \tag{19a}$$

[62]

which refines to

$$f(q,\tau) = 1 + \frac{1}{Y}\left(\sqrt{\frac{g_T^{(2)}(q,\tau) - 1 - \sigma_I{}^2}{\beta} + 1} - 1\right) \tag{19b}$$

when the instrument coherence factor β is taken into account [88].

In these equations,

$$Y = \frac{\langle I(q)\rangle_E}{\langle I(q)\rangle_T} \tag{20}$$

and $\sigma_I{}^2 = \sigma_{I,obs}{}^2/\beta = g_T^{(2)}(q,0) - 1$ is the initial amplitude of the single-recorded time-averaged ICF [62].

In classical solids, in classical liquids, and in gels, $f(q,0) = 1$. In pure solids, $f(q,\tau)$ does not decay. In pure liquids, $f(q,\tau)$ decays to zero by an exponential function similar to that of Eq. (16). In gels, $f(q,\tau)$ decays to a constant non-zero limit, $f(q,\infty)$, which provides a measure of the "frozen" fraction [83], in the form of

$$f(q,\tau) = \exp\left(-q^2\langle\delta^2\rangle\left(1 - \exp\left(-\frac{Dq^2\tau}{q^2\langle\delta^2\rangle}\right)\right)\right) \tag{21}$$

with $\langle\delta^2\rangle$ the mean-square displacement of the local fluctuations. A short-time linear approximation of this decay is

$$f(q,\tau) = 1 - Dq^2\tau + \ldots \tag{22}$$

In these latter equations, D is a collective diffusion coefficient describing the temporal decay of the density correlations. It was introduced in a 1973 seminal paper by Tanaka, Hocker, and Benedek, which treated gels as viscoelastic media with scattering that reflects thermally excited density fluctuations subject to damping due to polymer–solvent friction along with longitudinal and traverse compression and shear [89]. This treatment establishes a fundamental relation between the gel characteristic parameters related to these motions:

$$D = K_{os} + \left(4/3\right)G/\zeta \tag{23}$$

where K_{os} is the osmotic bulk modulus, G the shear modulus, and ζ the polymer–solvent friction coefficient [89]. D is further related to the density correlation function according to

$$D = \frac{\int \frac{kT}{6\pi\eta r}\hat{g}(r)\,dr}{\int \hat{g}(r)\,dr} \tag{24}$$

[90,91]

When the spatial correlation function is approximated to be the same in a polymer semidilute solution and in a comparable gel in the form of

$$\hat{g}(r) = c\frac{\xi}{r}\exp\left(-\frac{r}{\xi}\right) \tag{25}$$

[90]

this yields the dynamic gel polymer-network correlation length:

$$\xi = \frac{kT}{6\pi\eta D} \tag{26}$$

It is a general difference between polymer solutions and gels that even though K_{os} is slightly larger in solutions than in gels [53,91,92], G is considerably larger in gels than in solutions. As a result, D is commonly faster in gels, as found by DLS and NSE studies [54,62,91,93,94]. However, if in such assessment no proper care is taken about the non-ergodicity of gels and if they are treated as liquid-like ergodic media by use of the classical Siegert relation [84] in the form of

$$g^{(2)}(\tau) - 1 = \beta\sigma_I{}^2 \exp\left(-2D_{app}q^2\tau\right) \tag{27}$$

[57,89]

an apparent diffusion coefficient will be obtained instead:

$$D_{app} = -\frac{1}{2q^2}\lim_{\tau\to 0}\frac{d}{d\tau}\ln\left(g_T{}^{(2)}(q,\tau) - 1\right) = \frac{Y}{\sigma_I{}^2}D \tag{28}$$

As $\sigma_I{}^2 = g_T{}^{(2)}(q,0) - 1 < 0$, it often follows that $D_{app} > D$, and this is more pronounced at greater restriction of the local fluctuations. Hence, inappropriate treatment of polymer gels as ergodic media might misindicate rapid local dynamics, which is actually an artifact of improper data analysis [83]. In this context, Pusey and van Megen commented on the former seminal paper by Tanaka, Hocker, and Benedek [89] that it had incorrectly assumed the scattering field to be a zero-mean complex Gaussian variable, which is valid for the full ensemble but not for a sub-ensemble probed in a single DLS experiment. They further comment that this misconception, however, did seemingly not cause serious problems such as incorrect estimation of high apparent diffusion coefficients, D_{app}, in experimental studies that adopted this early method, because such effects of non-ergodicity may not greatly influence the light scattering by gels composed of flexible chains with low crosslinking density.

In a second approach, Joosten, McCarthy, and Pusey caught-up upon the Pusey–van Megen method and discussed it in view of the intrinsic heterodyne overlay of both the scattering from thermal dynamic concentration fluctuations, $I_F(q)$, and that from time-constant spatial concentration inhomogeneity, $I_C(q)$, in a gel [62]. Based upon that, it was argued that

$$f_N(q,\tau) = 1 + \frac{1}{X}\left(\sqrt{g_T{}^{(2)}(q,\tau) - \sigma_I{}^2} - 1\right) \tag{29}$$

with

$$X = \frac{\langle I_F(q)\rangle_T}{\langle I(q)\rangle_T} = 1 - \sqrt{1 - \sigma_I{}^2} \tag{30}$$

As in the Pusey–van Megen approach, $f(q,\tau)$ can be linearly approximated as

$$f_N(q,\tau) = 1 - D_N q^2\tau + \ldots \tag{31}$$

where D_N is again a collective diffusion coefficient describing the temporal decay of the density correlations. This coefficient is related to its analogue from the Pusey–van Megen approach given in Eqs. (22) & (23), and also to the apparent coefficient that is obtained if the data are treated by application of the classical Siegert relation [84] in the form of Eq. (27), by the relation

$$D_N = \frac{Y}{X}D = \frac{D}{1 - f(q,\infty)} = \frac{\sigma_I{}^2}{X}D_{app} = (2 - X)D_{app} \tag{32}$$

[57,62]

Joosten and co-authors commented that the results obtained from their partial heterodyne approach differ from their counterpart from the Pusey–van Megen approach, because the latter method properly accounts for the non-ergodicity caused by the static component by full-ensemble averaging of it (Eq. (20)), whereas the heterodyne approach relies on the simplifying assumption that static scatting contributions are much less relevant than dynamic contributions and can therefore be sufficiently taken into account by simple normalization to the long-time data recorded within the same single speckle (Eq. (30)). In their own words: "*in the heterodyne approach one assumes that the inhomogeneities do not constitute a relevant part of the gel system whereas in treating the gel as a general nonergodic medium one inherently takes into account all the features of the gel without making any assumptions as to what is relevant or irrelevant*" [62]. Despite this inaccuracy, however, Joosten and co-authors used their partial heterodyne approach to discuss DLS data obtained on poly(acrylamide) (pAAm) hydrogels, from which they derived fundamental conclusions such as showing that upon increasing the gel-network crosslinking density, the static parts of the scattering intensity increase considerably, whereas the dynamic parts are barely affected. This finding once more indicates that the dynamic fluctuations are the same in a solution and in a gel, whereas the static contribution is added on top of them in a gel, just as schematized in Fig. 6c and d.

Shibayama and co-workers [55,57,58] introduced a linearized variant of the latter equation in the form of

$$\frac{\langle I\rangle_{T,p}}{D_{app}} = \frac{2}{D_N}\langle I\rangle_{T,p} - \frac{\langle I_F\rangle_{T,p}}{D_N} \tag{33}$$

This equation allows the useful parameters D_N and $\langle I_F\rangle_T$, which is the time-average of the fluctuating part of the scattering intensity and further relates to the ensemble-average static part as $\langle I_C\rangle_E = \langle I\rangle_E - \langle I_F\rangle_T$ [19], to be derived from a single DLS experiment conducted at a single sample position p and first analyzed like an apparent ergodic medium to obtain the apparent diffusion coefficient D_{app} as a working variable.

In a later cooperative self-critical assessment, Moussaïd, Pusey, Slot, and Joosten used computer simulations to create virtual gels with different controlled degrees of connectivity and bond stiffness and simulated light scattering from them [95]. It was found that spatial inhomogeneity, as reflected by the static structure factor, is not simply coupled to non-ergodicity as derived from the dynamic scattering ICFs. Whereas strong bond stiffness always causes non-ergodicity, even at just little structural inhomogeneity, weak bond stiffness often entails little non-ergodicity even at comparably pronounced structural inhomogeneity. This notion is in agreement to an earlier statement by Pusey and van Megen, who stated that "*effects of [. . .] non-ergodicity may not greatly influence [the] light scattering properties in a gel composed of flexible polymers with low crosslinking density*", whereas in "*a gel made by linking relatively rigid fibers [. . .], effects of non-ergodicity [. . .] should be marked* [83]". The bond stiffness in the simulations by Moussaïd, Pusey, Slot, and Joosten was compared with that of stretched or destretched network strands in swollen or deswollen gels, suggesting the degree of gel swelling to be a strong factor of influence on the gel non-ergodicity. Some further years later, additional refinement to the preceding theories has been introduced by Furukawa and Hirotsu by taking into account dissimilarity of the dynamic fluctuations at different sample positions [96].

The main difference between the Pusey–van Megen non-ergodic medium method and the partial heterodyne method by Joosten et al. is that the non-ergodic medium method is based on regarding a permanent "frozen" component to *prevent* the full range of configurations to be realized in the speckle of observation (corresponding to the present sample orientation in the setup) within the time interval covered by the experiment, whereas the partial heterodyne approach suggests that this "dynamically uninteresting" [62] frozen fraction simply superimposes ("heterodynes") its scattering to that of the "interesting" dynamic fractions. Based upon that, different approaches of data normalization are taken in the two methods. The partial heterodyne method relies on a DLS

experiment conducted in just one speckle of the sample scattering and normalizes the ICF recorded in that speckle by its time-average asymptote according to Eq. (29), whereas the non-ergodic medium method performs this normalization of a single-speckle-recorded ICF by an ensemble-average intensity recorded in many different speckles (corresponding to many different sample orientations) according to Eq. (19), which is practically realized by either sampling and averaging the signal from a rotating cuvette in an independent experiment [62,87] or by translation of the sample during the DLS experiment itself and then factoring out the effect of this translation [97]. As a result, the intermediate scattering function, $f(q,\tau)$, that is derived from the ICF on the basis of these different normalization approaches is predicted to decay to zero in the partial heterodyne approach, whereas it is predicted to decay to a final non-zero value of $f(q,\infty)$ in the non-ergodic medium approach. In a later work by Manno and co-authors, the two methods were extended to allow for distinction between a fast fluctuating and a slowly relaxing contribution even when their respective timescales are not completely separated from one another [98].

To assess the utility of the Pusey–van Megen non-ergodic medium method and the partial heterodyne method by Joosten et al., Fang and Brown compared them on the basis of diverse experimental datasets [99]. This comparison revealed that the mathematics of data treatment plays a decisive role: whereas diffusion coefficients derived by the non-ergodic medium method are almost the same as those derived from the partial heterodyne method if inverse Laplace transformation is performed, incorrect diffusion coefficients are obtained by the Pusey–van Megen approach in a cumulant treatment, because the baseline has a strong detrimental influence in this case. This detriment was later addressed in an improved cumulant approach [100].

In another comparative work, Boger, Burchard and co-authors analyzed DLS data obtained on metal-ion crosslinked xanthan hydrogels with both the non-ergodic medium method and the partial heterodyne method [87]. In the case of a gel with completely non-moving randomly distributed scattering objects, the non-ergodic medium method was concluded to be more accurate than the partial heterodyne method, especially if the latter is based upon just one or a few large speckles in the scattering volume. By contrast, when the inhomogeneities are not fully frozen inside the gel but display some residual slow mobility, as it is the case in many supramolecular or transiently crosslinked polymer-network gels [101–104], the non-ergodic medium approach inaccurately lumps them into the immobile fraction, thereby overestimating it.

A third report aiming to compare the different methods of non-ergodic DLS data evaluation was published by Dogu and Oppermann [105], focusing on thermo-sensitive pNIPAAm hydrogels and aqueous solutions probed at different observation temperatures by both SLS and DLS. The thermal fluctuations isolated from the DLS data were found to be the same with both the non-ergodic medium method and the partial heterodyne method, and on top of that, this was further found to be the same as the plain-thermal scattering probed on uncrosslinked solutions by SLS. This systematic comparison justifies the applicability of the Debye–Bueche approach of SLS data evaluation, which explicitly relies on the assumption that the thermal fluctuations in kindred polymer solutions and gels are the same. By contrast, earlier studies by Hecht, Geissler, and different co-authors indicated the thermal scattering from gels to be slightly stronger than that from solutions [54,106]. The difference in these findings may be because the latter studies rely on generally less inhomogeneous gels made by end-linking or random side-linking of pre-polymerized building blocks, as shown in Fig. 1b and c, whereas the studies by Dogu and Oppermann are based on stronger inhomogeneous gels formed by free-radical crosslinking copolymerization, as shown in Fig. 1a. Fundamental difference in the extent of inhomogeneity in such different gels has been revealed by Liu and Oppermann [93], who related it to poorly efficient chain crosslinking and nanogel cluster formation in free-radical crosslinking copolymerization in contrast to better efficient and less inhomogeneous crosslinking in gels prepared from semidilute solutions of macromolecular precursors. A similar report has also been made by Ngai, Wu, and Chen [107], who attributed gel inhomogeneity and non-ergodicity in light scattering to stem from large and immobile voids in the network phase that span themselves between regions of dense-crosslinked clustered and loose-crosslinked inter-cluster domains. In view of pNIPAAm gels, such voids have been widely discussed in terms of local microphase-separation in the gel-network phase [43,46]. As a result, the different extent of overlay of (i) spatial crosslinking inhomogeneity in the form of nanogel-clusters plus potential additional voids in the gel-network phase, and (ii) inherent "frozen concentration fluctuations" in these different types of gels may lead to markedly different extent of static scattering caused by it, and potentially also to different accuracy of its isolation from DLS data.

3.2. Small-angle X-ray and neutron scattering

Scattering methods naturally probe structures on scales related to that of the scattered radiation wavelength. Hence, whereas light scattering addresses the regime of several tens or hundreds of nanometers, a complement is delivered by scattering of shorter-wavelength X-ray and neutron beams. In addition, X-ray and neutron scattering introduces further mutual complementarity due to their different nature of interaction with matter: whereas X-rays interact with electrons and reflect their density and contrast fluctuations in a sample, neutrons do so with nuclei. This principle allows the utility of these methods to be enhanced by selective labeling of selected parts of the sample, for example, by selective deuteration of the solvent, the polymer, or just parts of the polymer [26].

Like in the different modes of analysis discussed for light scattering, small-angle X-ray and neutron scattering (SAXS and SANS) data are commonly evaluated by fitting to a sum of two terms:

$$I(q) = I_{\text{liquid-like}}(q) + I_{\text{solid-like}}(q) \tag{34}$$

Most usually, the first term in Eq. (34) is an Ornstein–Zernike-type Lorentzian to account for scattering due to liquid-like concentration fluctuations on small scales (high q), reflected by a thermal osmotic correlation length ξ [77,90] as shown in Fig. 5b.

$$I_{\text{liquid-like}}(q) = \left(\rho_{\text{polymer}} - \rho_{\text{solvent}}\right)^2 \frac{kT\phi^2}{M_{\text{os}}} \cdot \frac{1}{1+q^2\xi^2} \tag{35}$$

In Eq. (35), ρ_{polymer} and ρ_{solvent} denote the scattering length densities of the polymer and the solvent, the difference of which is commonly termed contrast factor. ϕ is the polymer volume fraction, and M_{os} refers to the longitudinal osmotic modulus, which is related to the osmotic compression modulus, $K_{\text{os}} = \phi\,\delta\prod/\delta\phi$, and the shear modulus, G, by the relation $M_{\text{os}} = K_{\text{os}} + (4/3)G$ [89], thereby matching K_{os} in case of vanishing crosslinking density. In a rich series of contributions, Mallam, Horkay, Hecht, Geissler, and several co-authors checked on the utility of this equation for scattering-data fitting in relation to independent estimates of the moduli in it, as discussed in detail in Section 4 of this article. Note that in some other publications, a variant of Eq. (35) is employed that features an exponent different than 2 in the $(q\xi)^2$ term, depending on the solvent thermodynamic quality along with the polymer-chain constitution [108], and on potential further inter-chain interactions such as hydrogen bonding [76].

The second term in Eq. (34) accounts for additional excess forward scattering due to static concentration fluctuations on large scales (low q), reflected by a mean-square concentration-fluctuation amplitude $\langle c^2 \rangle$ spanning an inhomogeneity correlation

length Ξ, as shown in Fig. 5c. This second term distinguishes a crosslinked polymer-network gel from a non-crosslinked semidilute polymer solution; it arises due to the chain crosslinking that entails a frequency-independent plateau shear modulus, thereby no longer allowing concentration fluctuations (and hence, fluctuations of the local osmotic pressure) to equilibrate with time [26,75,106]. Two variants of the second term have been published.

One variant is a Guinier-type term [75,76,106,109] based on assumption of a Gaussian spatial concentration polydispersity [106], the spatial Fourier transform of which gives [75]

$$I_{\text{solid-like}}(q) = \left(\rho_{\text{polymer}} - \rho_{\text{solvent}}\right)^2 \langle c^2 \rangle \Xi^3 \exp\left(-q^2 \Xi^2\right) \tag{36}$$

thereby relating the inhomogeneity correlation length Ξ to a Guinier radius of gyration, $R_g = 3^{1/2}\,\Xi$ [76].

A second variant is a squared Lorentzian [26,52,54,56] as introduced in the Debye–Bueche formalism of scattering by microphase-separated solids with sharp internal interfacial boundaries [64–66], which applies to inhomogeneous media in general:

$$I_{\text{solid-like}}(q) = \left(\rho_{\text{polymer}} - \rho_{\text{solvent}}\right)^2 \frac{8\pi \Xi^3 \langle c^2 \rangle}{\left(1 + q^2 \Xi^2\right)^2} \tag{37}$$

This variant is closely connected to the popular Panyukov–Rabin theory, which is a specific model for gel polymer-network inhomogeneity that is often used to perform data fitting with formulas of the type of Eq. (7), related to that of Eq. (37) [56,69,72].

The contrast factor, Δρ, is in front of both the above summands, $I_{\text{liquid-like}}$ and $I_{\text{solid-like}}$, because both these scattering contributions arise from polymer concentration fluctuations in the gel, either caused by osmotic solution-like fluctuations on a scale ξ or by "frozen" solid-like fluctuations on a scale Ξ.

As a third variant for the second term, power-laws denoting interfacial scattering from mass-fractal structures at low q have been used in some publications [23,44,52,108,110].

4. Polymer-network inhomogeneity as studied by scattering experiments

The set of static and dynamic scattering methods reviewed in the preceding section has contributed a wealth of insight into the emergence, the effect, and the evolution of nano- and micrometer-scale structural complexity in polymer-network gels.

Early studies conducted by Shibayama, Norisue, and different co-authors were targeted at delivering fundamental insight into the interplay of the static and dynamic contributions to the scattering from gels. For this purpose, these researchers conducted DLS on thermo-sensitive poly(*N*-isopropylacrylamide) (pNIPAAm) hydrogels prepared and probed at different temperatures [19]. In these studies, the scattering intensity of the time-constant component, $\langle I \rangle_C$, was found to increase with T_{prep}, whereas that of the dynamic fluctuating component, $\langle I \rangle_F$, was found to be independent of T_{prep}. In an earlier study by Tanaka and co-workers [15], the same finding was attributed to different extent of critical dynamic concentration fluctuations during the gelation process that get "frozen" to becoming static inhomogeneites at the gel point. These pre-gelpoint dynamic fluctuations, and the post-gelpoint static inhomogeneity that results from them, are stronger if the gelling system is closer to its spinodal line when it approaches and passes the gelpoint, which is the case at high T_{prep} for a system with a lower critical solution temperature (LCST) such as pNIPAAm in water. A consistent obverse finding was reported for SLS and DLS studies on UCST-type polyacrylamide (pAAm) hydrogels by Takata, Norisuye, and Shibayama [85] and by Moussaïd, Slot, and Joosten [18]. In the latter, isolation of the fluctuating component from the scattering data on basis of the Pusey–van Megen approach showed that it is indeed a replica of the dynamic fluctuations in the pre-gel polymer system, which become frozen at the gelpoint. In pAAm hydrogels, these fluctuations are stronger at lower temperature, reasoned on the basis of the UCST-type miscibility of pAAm and water. In further line with this argument, $\langle I \rangle_F$ of LCST-type pNIPAAm hydrogels, which is independent of T_{prep}, increases with the temperature at observation T_{obs} [19]. Surprisingly, however, along with this increase of $\langle I \rangle_F$ with T_{obs} comes a closely coupled increase of $\langle I \rangle_C$ with T_{obs} as well [19,58]. This finding was also reported by Dogu and Oppermann [105], who explained it by suggesting locally dense-crosslinked domains to deswell more than locally loose-crosslinked domains upon worsening of the solvent quality. This was attributed to be the case because a decrease of the osmotic pressure that comes along with worsening of the solvent quality is more effective in dense-crosslinked polymer-rich regions with a per-se higher value of this quantity. As an alternative to this rationale, another argument may be that the solvent quality is generally lower in dense-crosslinked local domains than in loose-crosslinked local domains [18,44,45,62,75,111]; as a result, local dense-crosslinked regions are always closer to the critical theta-state than local loose-crosslinked regions, which is exacerbated upon raise of T_{obs} in an LCST system. Upon swelling in an excess good-solvent medium, however, opposing effects are observed for the static and dynamic parts of the scattering: whereas $\langle I \rangle_C$ is enhanced due to unravelling of static inhomogeneities as schematized in Fig. 3 and reported on specifically in seminal work by Geissler, Horkay, and Hecht [106,112], $\langle I \rangle_F$ is reduced due to a simple dilution effect [71]. It may be that this ambivalent effect of swelling causes a loss of the ability of the otherwise quite successful Panyukov–Rabin framework to fit the marked low-q upturn of the scattering intensity, thereby being in just partial quantitative agreement to experimental data recorded in this regime [56,72].

A later study by Furukawa and co-workers refined the preceding view on the role of swelling on the different scattering contributions in a set of inhomogeneous pAAm hydrogels, based on a conceptual picture of these gels to be composed of an assembly interconnected nanogel clusters [70]. At low polymer concentration, just a few nanogel clusters are present that are just loosely interconnected by a few chains. As a result, swelling pronounces the spatial inhomogeneity on scales of 10–100 nm, as quantified by static light scattering, and it broadens the mesh size distribution on scales of 1–10 nm, as derived from the dynamics of network-strand fluctuation assessed by DLS, both schematized in the left half of Fig. 8a. At high polymer concentration, by contrast, many nanogel clusters are present that are interconnected by many chains. As a result, strong scattering is contributed by these nanogels in both deswollen and swollen states, but swelling homogenizes the mesh size distritubion, as shown in the right half of Fig. 8a. At intermediate concentrations, the structure is an intermediate of these two and therefore less inhomogeneous. When assessed in a systematic fashion, it was found that increase of the polymer concentration or volume fraction monotonically decreases the dynamic part of the scattering in both deswollen and swollen states, as shown by the lowermost dataset in Fig. 8b; this is in agreement to the related finding by Shibayama et al. [71]. The dynamic part, however, displays a minimum at intermediate concentration, in agreement to the above rationale, and it is pronounced by swelling, as seen from the middle and upper dataset in Fig. 8b. Whereas the swelling-related finding is in agreement to the work by Shibayama et al. [71], the finding of a minimum at intermediate concentration is not.

Related to the preceding fundamental investigations, other early studies by Mallam, Horkay, Hecht, Geissler, and several co-authors delivered further conceptual insight into the dynamic liquid-like and the static solid-like scattering contributions in polymer-network gels. These studies also substantiated the utility of the equations listed in the preceding section to account for the different scattering contributions, and furthermore, the quantitative

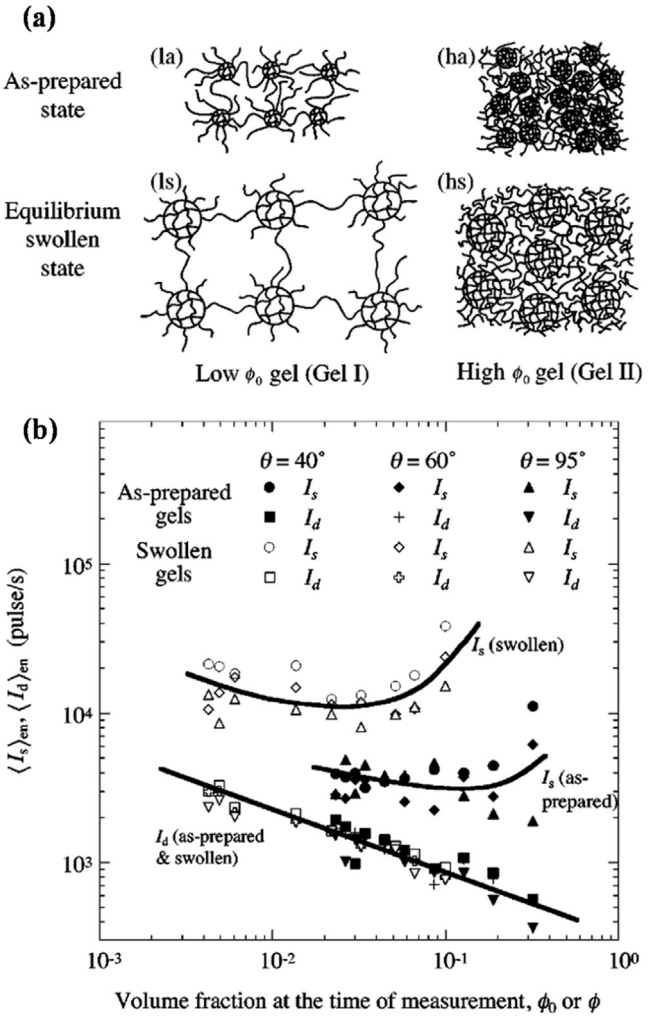

Fig. 8. Conceptual pictures (a) and scattering data (b) of Furukawa and co-workers to investigate the role of swelling on the interplay of static and dynamic scattering contributions of inhomogeneous hydrogels, based on a conceptual picture of these gels to be composed of an assembly interconnected nanogel clusters. (a) Schematics of inhomogeneous polyacrylamide (pAAm) hydrogels prepared at low (left side) or high (right side) monomer concentration, sketched in a state of preparation (upper row) and after swelling (lower row). (b) Static and dynamic parts of the ensemble-averaged scattering intensity, $\langle I_s \rangle_{en}$ and $\langle I_d \rangle_{en}$, as a function of the volume fraction of monomeric repeat units at the time of measurement, denoted by ϕ for swollen gels (open symbols) and ϕ_0 for gels probed in a state as prepared (closed symbols). [70], Copyright 2003.

Reproduced with permission from the American Physical Society.

relation of the parameters contained in them to the gel structures and thermodynamics [21,23,26,44,45,75,106,109,110,112]. In one series of studies, for example [44,45], pAAm hydrogels prepared at 8% (w/w) monomer concentration with crosslinker contents of 0.1–0.5% (w/w) were probed by osmometry, rheology, dynamic light scattering, and small-angle X-ray scattering (SAXS), and an increasing discrepancy between the longitudinal osmotic modulus determined from swelling experiments and from dynamic light scattering data was found. This discrepancy arises due to concentration fluctuations with a mean-square amplitude of $\langle c^2 \rangle$ in the sample, which occur due to static inhomogeneity in the sample that is stronger at higher crosslinker content. Quantification of $\langle c^2 \rangle$ by SAXS within the framework of Eq. (36) quantitatively explains this discrepancy. In a related work, Cohen and co-workers illustrated pAAm hydrogels prepared at 10% (w/w) monomer concentration with crosslinker contents of 1–9% (w/w rel. to the monomer) [113] to consist of densely crosslinked nanogel clusters embedded in a loosely crosslinked background. Small-angle X-ray scattering (SAXS) analyses and data-fitting with combined Lorentzian and Gaussian terms denoted an Ornstein–Zernike-type correlation length, ξ, interpreted to reflect the polymer-network mesh size, to increase with increasing crosslinker content, whereas a Guinier radius, R_G, interpreted to reflect the radius of local dense-crosslinked nanogel clusters, decreases with increasing crosslinker content. This finding was explained by a decrease of the solvent quality of the aqueous medium at higher crosslinking density, in agreement to other reports [18,44,45,62,75,111], thereby leading to shrinkage of the clusters and, in turn, expansion of the surrounding loosely crosslinked network meshes

Another set of fundamental studies was conducted by Bastide, Mendes, Boué, and different co-authors, mostly focusing on poly(dimethylsiloxane) (pDMS) networks and gels prepared by polymer end-linking [25,92,114–116]. In a simplistic view, when SANS is conducted on uniaxial stretched samples, it may be expected that the scattering intensity should decrease in the stretching direction due to simple dilution of the polymer-segmental density by the stretching. In contrast to this simple expectation, however, the opposite of an *increase* of the scattering intensity in this direction was found. This effect, commonly referred to as the "abnormal butterfly pattern" [116,117], was investigated by Rouf-George, Bastide, Munch, and co-workers [25,114] through the use of SANS and DLS conducted in a scanning mode, revealing that the enhancement of the SANS intensity in the uniaxial stretching direction is due to amplification of its static rather than its thermal scattering contributions. It can therefore can be viewed to originate from anisotropic enhancement of spatial network inhomogeneity in the stretching direction [118]. Later on, the "abnormal butterfly pattern" and the related phenomenon of strong enhancement of the forward excess scattering at low q by isotropic swelling [24,108] was assessed in an extensive series of systematic SANS experiments. These were conducted on polystyrene network-gels crosslinked in a random pattern by polymer-analogous Friedel–Crafts reactions [91,116] and on pDMS gels prepared by different methods [25], each probed at different degrees of swelling and stretching. This and another series of studies showed that random crosslinking in "*a reaction bath well in the semidilute regime*" [24] is crucially necessary to show the above effects of weak scattering in the state of gel preparation but strong scattering after swelling (cf. Fig. 3) or stretching, whereas gels formed by end-linking of just short oligomeric chains at a level of dilution that does not allow for chain overlap forms strongly inhomogeneous structures at both the preparation and at post-preparation excess swollen states [41,115], as comprehensively reviewed by Bastide and Candau [59].

The preceding survey shows that the analytical or phenomenological functions for the static and dynamic scattering contributions from polymer-network gels given by Eqns. (1–10), (19), (29), and (34–37) are a good fit. Based on that, Okay, Oppermann, and several co-authors used the Debye–Bueche method of data evaluation to quantify the polymer-network inhomogeneity in the form of the mean-square static fluctuation of the refractive index in the gel, $\langle \eta^2 \rangle$, and related this parameter to the impact of several variables during the gel preparation, including the monomer and crosslinker concentrations [35,36,38,67–72] and reactivities [37,40,73,74], the gel preparation temperature [72], and the rate of the gelation reaction [39]. Several studies by Okay and co-workers led to the finding that the gel inhomogeneity is more pronounced at higher crosslinker contents; these studies also indicated a correlation of stronger gel spatial inhomogeneity, as assessed by $\langle \eta^2 \rangle$, to weaker gel elasticities, as assessed by the ratio between the ideal and the real elastic modulus [35,38,67]. This finding is explainable on basis of a conceptual picture presuming extensive cyclization, multiple crosslinking, and growth of nanogel clusters during the gelation

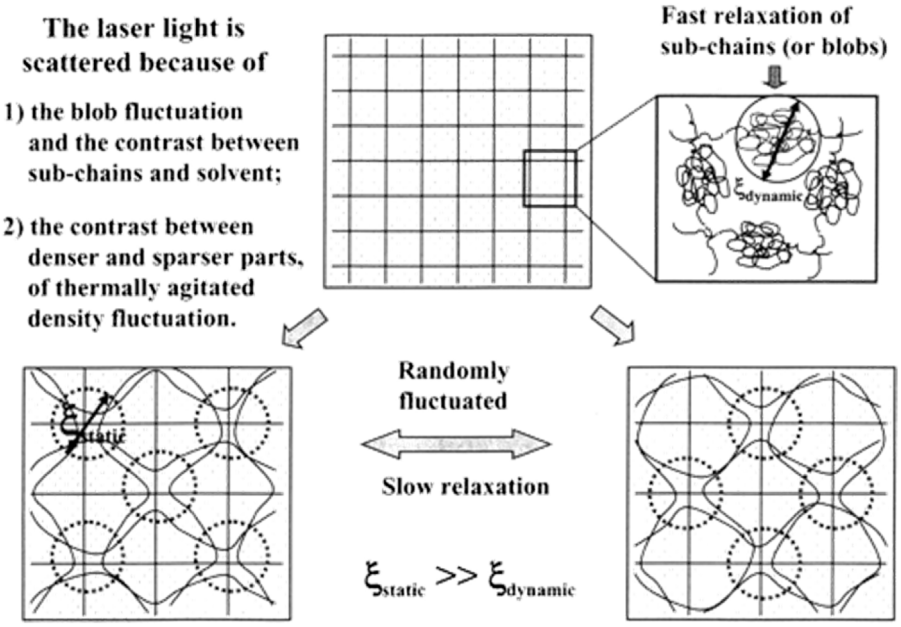

Fig. 9. Schematic of fast and slow relaxation modes of a uniform gel network swollen in good solvent. [107], Copyright 2004. Reproduced with permission from the American Chemical Society

process at high crosslinker content. When shedding a detailed look on this, however, Okay reported a non-monotonous increase of the gel inhomogeneity with the crosslinker content, climaxing in a threshold of 9% crosslinker, above which markedly heterogeneous porous gels are obtained. In the same context, Kizilay and Okay also showed that pAAm gels prepared with the aid of *N*,*N*,*N*',*N*'-tetramethylethylenediamine (TEMED), which acts as both a catalyst for polymerization-initiation and as a base, age towards a more homogeneous nanostructure when left in their scaffolding light-scattering cuvettes over a period of 60 days. This finding was explained by presumption of hydrolysis of the acrylamide (AAm) groups to deprotonated acrylic-acid (AAc) groups, leading to expansion of local dense domains inside the gel that occurs on cost of compression of local loose domains in the gel, thereby homogenizing its static concentration fluctuations [35]. Kizilay and Okay supported this assumption by quantification of the expected change of the root-mean-square refractive-index fluctuation in the gel, which they confirmed by static light scattering and data evaluation by the Debye–Bueche method.

In a further study, Orakdogen, Kizilay, and Okay conducted reaction-time-dependent static light scattering experiments on rapidly polymerizing acrylamide (AAm) and on slowly polymerizing *N*,*N*-dimethylacrylamide (DMAAm) monomer solutions. They found that the scattering intensity, which reflects the sample concentration-fluctuation inhomogeneity, evolves in three stages. First, it increases due to continuous formation of spatially isolated polymer coils in the dilute state. Then, it reaches a maximum as the polymerizing solution reaches the chain-overlap threshold. Finally, the scattering intensity re-decreases upon further polymerization, which is due to screening of local concentration fluctuations by the steady further increase of the overall polymer concentration in the system [37]. Depending on how soon or late the gelpoint fixes the remaining concentration inhomogeneity, the resulting polymer-network gels are homogeneous (late gelpoint, DMAAm system) or inhomogeneous (early gelpoint, AAm system.) Copolymerization of these different monomers with one another in additional presence of a crosslinker yields more homogeneous and mechanically stronger gels at higher content of the slowly polymerizing DMAAm monomer, again interpreted by its action of delaying the gelpoint to higher conversion [40]. This conclusion was drawn from SLS and DLS analyses, denoting the gels to display lower $\langle\eta^2\rangle$ and $\langle I\rangle_C$ at higher DMAAm comonomer content, along with exhibiting smaller ξ_{SLS}, as derived from Debye–Bueche analyses, and ξ_{DLS}, as derived from the cooperative diffusion coefficient by Eq. (26), which was both interpreted to reflect a smaller mesh size and higher crosslinking density in the gels, in agreement to their equally higher elastic moduli as determined by rheology.

As an alternative to gel formation by crosslinking copolymerization of monomers and crosslinkers, Liu and Oppermann prepared polystyrene gels by polymer-analogous interconnection of pre-polymerized crosslinkable chains from semidilute solutions. These gels were found to exhibit much more homogenous structures than comparable gels prepared by crosslinking copolymerization, as assessed by static light scattering and data evaluation by the Debye–Bueche method. In particular, a lower threshold for macroscopic gelation was found at that concentration at which the room-mean-square concentration fluctuation in the gel, $\langle c^2\rangle^{1/2}$, equals its average concentration, *c*, that is simply given by the overall mass of polymer per overall volume of the gel [93]. Related to this study, Ngai, Wu, and Chen [107] prepared poly(methyl methacrylate] (pMMA) gels by random crosslinking of pre-polymerized chains in a semidilute solution by dimerization of photoreactive sidegroups that are attached to the precursor chains in a random pattern. This approach allowed the same system to be transferred from a sol state to a gel state with the ability to interrupt the reaction at will. During such interruption, DLS was conducted. It was found that both the pre-gel solutions and the gels obtained from them display full relaxation of the intermediate scattering function, $f(q,\tau)$, thereby denoting both the solutions and the gels to be ergodic. This relaxation displayed two modes in each case, a fast and a slow one, both found to be diffusive with scaling of $\tau \sim q^{-2}$. The fast mode was attributed to reflecting fluctuations of the network-strands between two adjacent crosslinking junctions, as shown in the upper part of Fig. 9, whereas the slow mode was interpreted to reflect density fluctuations on 100-nm scales that occur by correlated motion of crosslinked domains in the network, as shown in the lower part of Fig. 9. According to the authors, such diffusive motions are still possible in gels, even though they require comparably long

times of several seconds, but when given this time, the system is ergodic. The authors commented this finding of ergodicity to be actually expectable, because a usual light scattering probe volume has a size of several hundred micrometers and therefore contains a multitude of 10–100-nm sized nanogel clusters, such that speckles probed at different locations in the sample should be equal. Based on this argument, the very common opposite finding in many gels was attributed not to stem from densely crosslinked local clusters but from large and immobile voids in between them, which are formed in chain-growth gelation processes such as those based on harsh free-radical crosslinking copolymerization but which can be absent in gentle bond-percolation-type polymer-analogous gelation of pre-polymerized macromolecular precursors. The basis for this finding is an earlier study by Zhao, Zhang, and Wu that focuses on light scattering on differently jam-packed nanogel (50–100 nm) suspensions [119]. Inhomogeneity and non-ergodicity in these systems was attributed to inter-nanogel voids that form if the system gels faster than diffusive relaxation of the nanogels can occur. This conceptual picture is in agreement to another study by Grube and Oppermann, who prepared polyethgylene glycol (pEG) hydrogels by controlled thiol–ene interconnection of end-functionalized linear and star-shaped building blocks, according to the schematic in Fig. 1c, in comparison to polyacrylamide (pAAm) gels prepared by uncontrolled free-radical crosslinking copolymerization of acrylamide (AAm) and *N*,*N*'-methylenebisacrylamide (BIS) according to the schematic in Fig. 1a [34]. Light scattering denoted the pEG gels to be more homogeneous than the pAAm gels in their states of preparation. This finding was explained by considering that chain growth in the process of free-radical crosslinking copolymerization of AAm and BIS requires diffusive mass transport of the monomers to the poorly mobile growing chains and clusters, whereas step-growth branching of the thiol–ene-functionalized pEGs occurs by bond percolation of adjacent oligomeric building blocks without necessity for extensive mass transport. As a result, stronger inhomogeneity of the polymer segmental density is present in the pAAm than in the pEG gels, manifesting itself in stronger light scattering intensities in the gel states of preparation. After swelling, however, both these types of gels were found to display similarly strong inhomogeneity, which was also found for poly(styrene-*co*-maleic anhydride) organogels crosslinked by ethylene glycol in a semidilute solution upon post-gelation swelling in dioxane [63]. These results are addressable to the notable unravelling of network connectivity defects by inhomogeneous swelling that they cause, as also studied systematically for defect-controlled tetra-pEG gels and shown schematically in Fig. 3 [41]. Hence, even though Grube and Oppermann concluded their paper with the pessimistic phrase "*there seems to be no clear correlation between whatever kind of inhomogeneity and network imperfections*", it finds itself in sound logical agreement with several complementary reports, as just discussed.

To systematically address and challenge the statistical-mechanical Panyukov–Rabin model, a series of studies conducted by Shibayama and various co-authors focused at its prediction of a crosslink saturation threshold. The core of these studies is a two-part report by Norisuye, Shibayama, and co-authors on small-angle neutron scattering (SANS) [16] and swelling experiments [17] conducted on pNIPAAm hydrogels either (i) made by free-radical crosslinking copolymerization of monomers and crosslinkers or (ii) made by γ-ray induced interconnection of pre-polymerized linear chains in semidilute solution. The type-(ii) γ-ray gels display much weaker low-*q* excess forward scattering in SANS than the type-(i) polymerized gels. From this finding, it was concluded that the type-(ii) gels display spatial inhomogeneity only due to fixed thermal concentration fluctuations during the γ-ray crosslinking, whereas the type-(i) gels display additional inhomogeneity due to presence of local dense-crosslinked nanogel clusters. Curve-fitting with a Panyukov–Rabin-based formula yields the average network-strand degree of polymerization in the gels, *N*, which approaches a limiting value of $N = 42$ at increasing crosslinking content in the type-(i) gels. This limit corresponds to a crosslinking-saturation threshold in quantitative agreement with the Panyukov–Rabin prediction. As the crosslinker content approaches this limiting value, the polymer-concentration correlation length derived from SANS diverges for the type-(i) gels, whereas it does not diverge for the more homogeneous type-(ii) gels. This latter result is in disagreement to the Panyukov–Rabin model, which is therefore found to give excellent predictions for the monomer-polymerized gels of type (i), but not for the γ-ray crosslinked gels of type (ii), even though this model was originally developed for exactly this type-(ii) sort of gel.

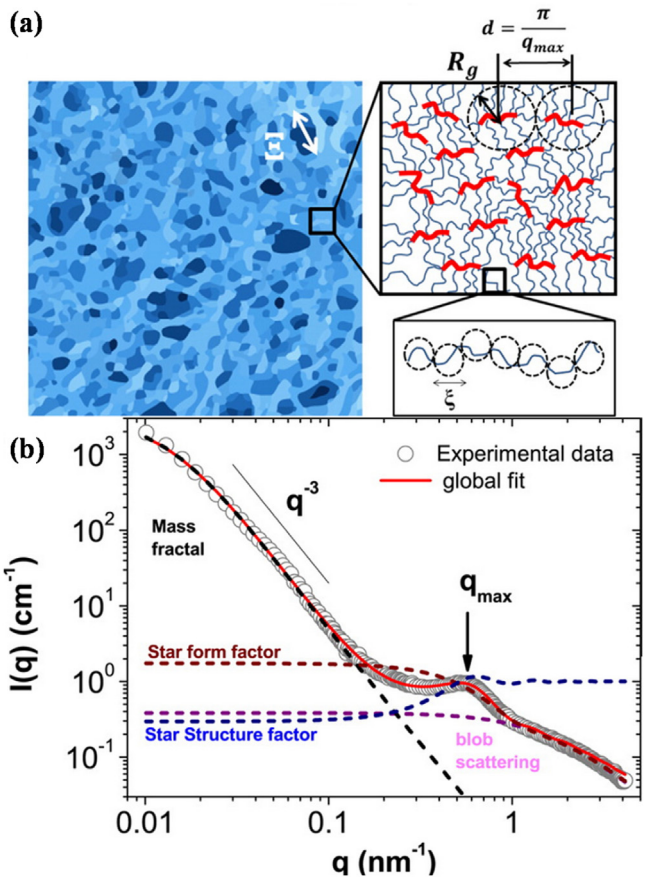

Fig. 10. Multi-scale nano- to microstructural complexity in hydrogels formed from poly(ethylene glycol)-diacrylate (pEG-DA) macromonomers and the respective contributions to small-angle neutron scattering, as reported by de Molina, Lad, and Helgeson [126]. (a) Schematic of the network structure on multiple scales, which is quantified by three parameters: the pore-void size on large scales, Ξ, the star-polymer radius of gyration, R_g, and the local correlation-blob lengthscale, ξ. (b) SANS data recorded on these gels reflect this structural complexity in the form of low-*q* mass-fractal scaling, a mid-*q* peak associated to the local star-polymer structures, and high-*q* Lorentzian scaling attributed to the local correlation-blob structure. Overlay of four individual terms to assess these structures gives a good global fit. [136], Copyright 2015.

Reproduced with permission from the American Chemical Society.

In a closely related study, Takata, Norisuye, and Shibayama also probed the type-(i) monomer-polymerized gels at different crosslinker contents and preparation temperatures by SANS [82]; later on, this was further supplemented by static light scattering (SLS) [42]. These studies show the above-discussed crosslinking saturation threshold to be reflected by power-law scaling of the *q*-dependent SANS intensity, whereas Lorentzian scaling is seen below the threshold, overlaid by additional diverging low-*q* excess forward scattering above the threshold. The crosslink sat-

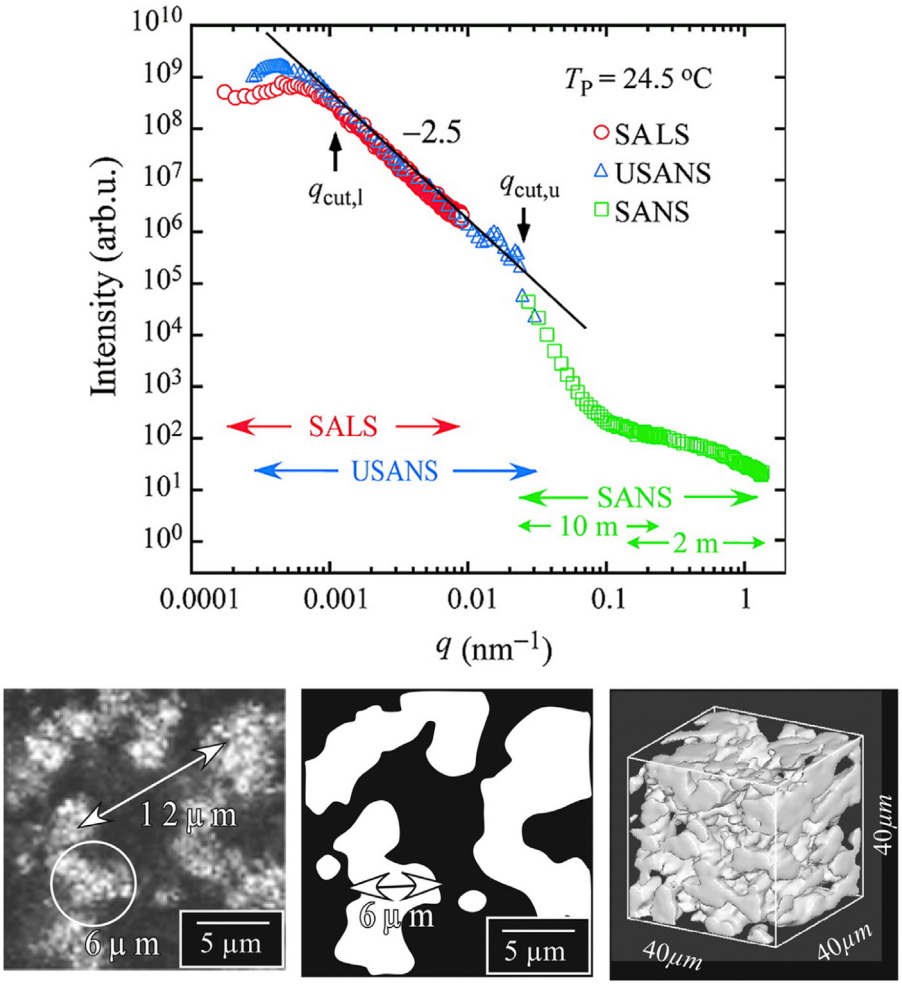

Fig. 11. Combined scattering data of a nano- and micrometer-scale inhomogeneous poly(*N*-isopropylacrylamide((pNIPAAm) hydrogel prepared at 24.5 °C, as obtained by small-angle light scattering (SALS), ultra-small-angle neutron scattering (USANS), and conventional small-angle neutron scattering (SANS). The lower panel displays supportive imaging data obtained by confocal laser scanning microscopy. The length indicated by the arrow corresponds to the spacing (12 μm) obtained from q_{max} in the SALS and USANS scattering profiles. Furthermore, the diameter of the circles indicates the $l_{cut,u}$ (≈6 μm) obtained from $q_{cut,l}$ in SALS and USANS scattering profiles. [46], Copyright 2008.

Reproduced with permission from the American Chemical Society.

uration threshold is reached at a low crosslinker content if the gel preparation temperature is high and vice versa. This relation is quantitatively substantiated in the form of $N(c_{x\text{-linker}}, T_{prep})$ as predicted by the Panyukov–Rabin theory, which was found to be in good agreement to experimental values of *N* obtained from further Panyukov–Rabin-based fitting of the SANS curves.

In a further follow-up work, Norisuye and co-authors probed the type-(ii) γ-ray crosslinked gels by dynamic light scattering and decomposed the scattering data into static and dynamic parts, $\langle I \rangle_C$ and $\langle I \rangle_F$, respectively, by use of different variants of the partial heterodyne method [60]. While $\langle I \rangle_C$ displayed considerable increase with the crosslinking density (varied by the γ-ray dose), $\langle I \rangle_F$ was found to be independent of it, but despite this independence, it was found to vary as a function of the sample position, which the authors denoted as "dynamic inhomogeneity". Correlation of $\langle I \rangle_C$ and $\langle I \rangle_F$ to one another revealed inverse proportionality. This finding is in agreement to the schematic in Fig. 6d: densely crosslinked domains are characterized by strong $\langle I \rangle_C$ but strongly suppress chain-segmental fluctuation, which corresponds to weak $\langle I \rangle_F$, and vice versa. A theoretical treatment of this dissimilarity of the dynamic fluctuations at different sample positions has been reported by Furukawa and Hirotsu two years before [96].

Further consistent agreement to the Panyukov–Rabin model has been demonstrated in another series of work by Ikkai, Shibayama and collaborators in view of a phenomenon referred to as the anomalous crosslinker-dependence. In these investigations, p(NIPAAm-*co*-AAc) gels prepared at different crosslinking degrees were probed by dynamic light scattering and small-angle neutron scattering (SANS) [16,32,78–81]. If the observation temperature is below the polymer-hydrogel LCST, stronger inhomogeneity is observed at higher crosslinker content. By contrast, if the observation temperature is higher than the polymer-hydrogel LCST, the opposite effect of a *lower* scattering intensity at higher crosslinker content [78,81] is found. This finding was explained by considering the inhomogeneity at low observation temperature to be mainly reflected by static concentration fluctuations in the gel, which are stronger at higher crosslinker content, up to causing divergence of the structure factor and low-*q* SANS intensity beyond a crosslink saturation threshold [78,79]. By contrast, *dynamic* critical fluctuations provide the main contribution to the scattering intensity at high observation temperature, manifesting themselves in the form of a correlation peak in the *q*-dependent structure factor and SANS intensity [16,32,79,80]. These fluctuations are suppressed in the case of strong gel crosslinking, causing lower scattering intensities and attenuation of the SANS correlation peak

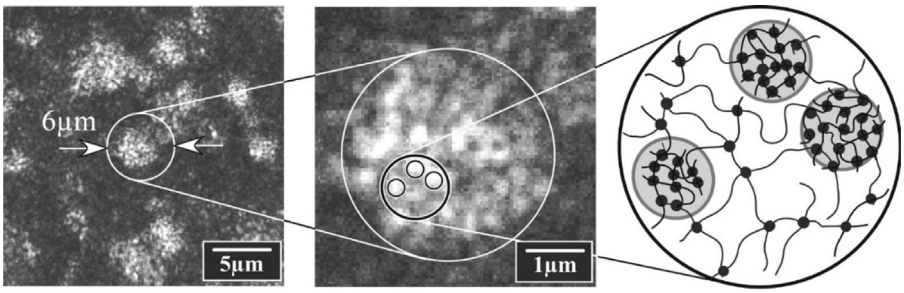

Fig. 12. Deeper confocal-microscopy analysis of the bi-continuous microphase-separated hydrogel structure shown in Fig. 11 and interpretation of it as a loose-connected assembly of locally tight-crosslinked microgel clusters, as sketched on the right. [46], Copyright 2008.
Reproduced with permission from the American Chemical Society.

at high crosslinker content. These findings have been denoted to be in striking agreement to a variant the Panyukov–Rabin theory for weakly charged gels [30], which quantitatively predicts the experimental scattering observations [78–80]. Closely similar results and similar agreement to the same theory were also reported for poly(*N*-isopropylacrylamide-*co*-acrylamido-2-methyl-1-propane sulphonic acid) (p(NIPAAm-*co*-AMPS) gels [120]. In a further variant of this series of work [121], SANS was conducted on related gels either grown from NIPAAm and AAc monomers or prepared by UV-irradiation of pre-polymerized chains, thereby exhibiting either random or segregated nanometer-scale distributions of their chargeable AAc groups. As in the preceding studies, a distinct correlation peak is observed in SANS at high observation temperatures, denting microphase-separation at the onset of gel collapse in agreement to the Rabin–Panyukov theory for weakly charged gels [30]. However, in the gels with inhomogeneous non-random AAc-group distribution, this peak is found to be sharper and localized at lower q, along with a generally stronger scattering intensity, than in the gels with random AAc-group distribution. All these observations indicate the solvent quality to be worse in the gels with locally segregated AAc-group distribution than in the gels with random AAc-group distribution [30], which is explainable by assumption of a lower effective charge degree due to stronger counterion condensation when the AAc groups are localized in segregated domains. This presumption is in agreement with further observation of less low-temperature swelling and lower gel volume phase transition temperatures in this variant of the gels.

Polymer-network inhomogeneity as characterized systematically in the numerous preceding references is usually attributed to be detrimental for the polymer-network properties, as it typically lowers their elastic moduli, entails turbidity, and complexes solute and tracer diffusive penetration [1,2]. Thus, attempts have been made to prepare homogeneous, defect-free networks for a long-time. Early attempts to reach this goal were based on end-linking of suitably functionalized precursor polymers [122], as shown in the lower half-panel of Fig. 1c. To assess the propensity of formation of inhomogeneity even in such a controlled approach, Urayama and co-workers prepared pDMS gels by end-linking either unimodal or bimodal fractions of intermediate or long-and-short precursor chains. SAXS studies on toluene-swollen samples revealed inhomogeneous nanostructures in both these types of gels, which was interpreted to stem from backbiting reactions according to the shortest-closed-circuit concept, thereby creating local defects and voids in the polymer networks [123]. In another study, even more severe inhomogeneity was found and interpreted to stem from aggregates of polymerized linker units [109].

More than twenty years later, Sakai, Shibayama, and collaborators presented an approach for formation of model-type networks by cross-coupling of two complementarily functionalized tetra-arm pEG building blocks [124] in aqueous solution, denoted tetra-pEG gels. When these precursor polymers are reacted with matched stoichiometry, homogeneous networks are obtained that display a sole-Lorentzian scattering profile in SANS, whereas at mismatched stoichiometry, the scattering profile is a linear combination of a Lorentzian and a star-polymer form factor, accounting for the still model-network-type gel fraction and the residual unconnected star-polymer sol fraction in a ratio determined by the stoichiometry mismatch [125]. This finding denotes tetra-pEG gels to be free of spatial polymer-network inhomogeneity, which is further supported by an additional finding of complete decay of their elastic incoherent structure factor (EISF) [126] in neutron spin echo experiments [94]. This quantity usually has a non-decaying part in conventional inhomogeneous gels, because their segmental mobility is constrained both in their densely crosslinked domains, where the network strands are confined within nanogel clusters, and in their swollen loose-crosslinked domains, where the network chains are strained. In tetra-pEG gels, by contrast, full decay of the EISF indicates the network-chains to be better mobile, which is argued to be because there is neither such kind of constraining spatial inhomogeneity. In the same study, it was also argued that in the high-resolution scattering range at $q\xi > 1$, where the defining length scale of the measurement is no longer the correlation length ξ but q^{-1}, transition from Zimm-mode segmental dynamics to collective-diffusion dynamics of the whole network-chains [89] occurs at lower q in tetra-pEG gels than in conventional gels. It was argued that this is because in addition to exhibiting no spatial inhomogeneity, tetra-pEG gels also exhibit no connectivity and topological inhomogeneity, such that they do not contain local small meshes thresholding the transition of segmental Zimm-dynamics to collective network-strand diffusion.

In contrast to these consistent findings of astonishing homogeneity on both small and large scales in neutron scattering, however, a later study [47] evidenced that tetra-pEG gels anyhow display an upturn of their scattering intensity in the low-q light-scattering regime that manifests itself in the form of an $I(q) \sim q^{-2}$ power-law when they are probed in a state of preparation. This type of scaling is not in agreement with the above equations for the solid-like inhomogeneity in usual SANS and SLS analyses, which predict steeper scaling with apparent exponents of 3–4. Instead, it can be interpreted to reflect a second, large-scale correlation length Ξ in the gels, in addition to their regular small-scale correlation length ξ. A possible cause for this bimodal nanostructure can be pEG–pEG supramolecular association, which has been shown to exist in uncrosslinked pEG solutions [127], causing an additional supramolecular crosslinking structure on top of the model-network covalent one. This line of argument is supported by the observation that the low-q upturn in light scattering vanishes upon swelling of the gels [47], which can be interpreted to break these presumed supramolecular crosslinks. In this limit, the gels are found

to reflect sole-Lorentzian scattering again. This is further found to be independent of the pEG precursor molecular weight, such that scattering curves obtained from different gels can be collapsed on a single mastercurve if reduced variables are employed in a plot of $I(q)/(\phi_0\,\xi^2)$ vs. $q\xi$.

In contrast to such reversible inhomogeneity, another recent work on a variant of tetra-pEG-type model networks reported SANS data with a steep power-law upturn at low q. These data were fitted to a broad-peak model that contains a power-law term to account for this low-q upturn and an extended Lorentzian term that accounts for two high-q structural features: a thermal correlation length, ξ, and an additional parameter reflecting the effective polymer-network mesh size, d. This mesh size was found to be larger than idealized from the star polymer-building block geometries due to network defects. The fitting values of d semi-quantitatively agree with estimates of the effective mesh size from swelling measurements analyzed with the classical Flory–Rehner theory within a factor of ~1.5–2. [128]. A related finding was also made on yet another variant of tetra-pEG gels, where SANS curves of samples formed from small building blocks in polar D_2O exhibited broad shoulders or even peaks in the mid-q region, which was addressed to clustering of the hydrophobic crosslinking-junctions formed by norbornene–thiol click-chemistry in this study [129]. Apart from this irregularity, however, the polymer-network mesh size was found to be in good agreement to expectations based on scaling arguments.

Other than the latter approaches of purposely preparing defect-free homogeneous gels, which attract attention in view of serving as a well-defined basis both to (re-)address fundamental polymer-physical questions [94,130–133] and to develop highly tough [134] or resilient [129] soft materials, many gels based on common materials such as the popular pEG-diacrylate macromonomers or the famous thermo-sensitive poly(*N*-isopropylacrylamide) [135] display the contrary of very complex nanostructures. This is a consequence of several different effects during the gel formation. First, the usual sources of inhomogeneity as described within the frozen-blob concept in the case of polymer-crosslinking or by different monomer and crosslinker reactivities in crosslinking copolymerization [2] are active. Second, on top of that, additional nanostructural complexity arises from inherent peculiarity of the material at hand. For example, Helgeson and co-workers [136] conducted a series of investigations on hydrogels formed from pEG-diacrylates (pEG-DA), which are a popular material in the biosciences. From SANS experiments, a structural model based on self-excluded, highly branched star polymers arranged into a fractal network with both small-scale polymer-network inhomogeneity and large-scale gel porosity was proposed, as shown in Fig. 10a. The primary implication of this structural picture is that polymer-network inhomogeneity in these gels arises not from crosslinking defects, but rather from an inhomogeneous distribution of the polymer concentration, as also shown in Fig. 10a. Based upon this model, a sophisticated multi-term function was derived to fit the SANS data, consisting of a universal mass-fractal term to assess the large-scale pore structure, and a set of system-specific terms to represent the local structure of mutually interconnected star polymers, as shown in Fig. 10b. Data fitting with this model allowed the void-volume fraction of the heterogeneous pore-structure on large length scales to be determined, revealing it to display a direct correlation to the modulus and crosslinking efficiency derived from rheology. In some relation to this, Chaieb and co-authors studied gelatin hydrogels crosslinked by either physical or chemical means or by both [108]. The low-q forward neutron scattering of the chemical gels in this study was fitted with a mass-fractal term and interpreted to reflect spatial inhomogeneity due to crosslinked aggregates, which was further interpreted to be responsible for non-affinity at large deformation. In another work, a similar interpretation of aggregated crosslinking-junctions was concluded from SANS on poly(vinyl alcohol) hydrogel membranes crosslinking by sulfonic-acid functionalized linkers, thereby forming ionic domains in the material that favorably support proton conduction [137].

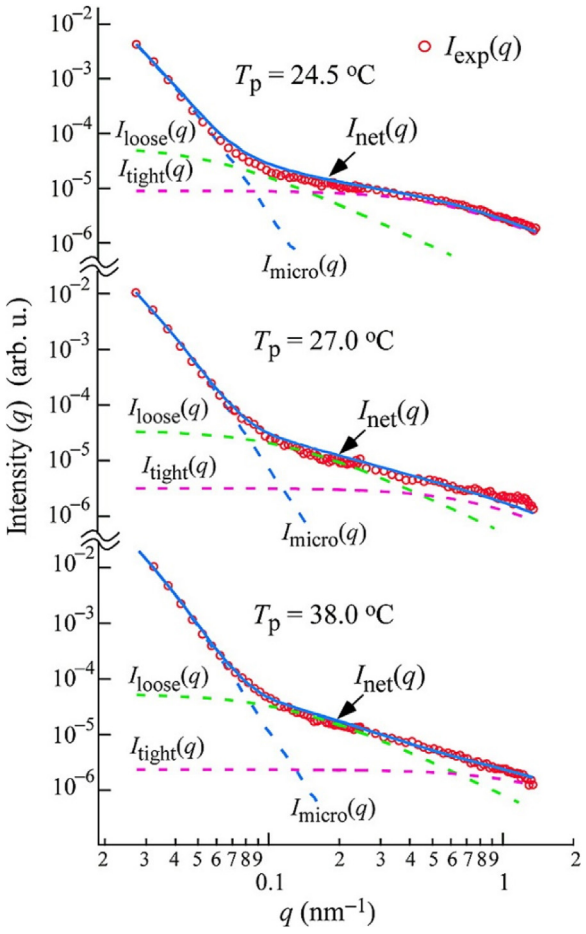

Fig. 13. Fitting of SANS data analog to those in Fig. 11, which belong to bi-continuous microphase-separated hydrogel structures as the one shown in Fig. 12, to a combined term of three Lorentzian profiles denoting the microgel-internal tight crosslinking, $I_{tight}(q) = k_{tight}(1 + q^2\xi_{tight}{}^2)^{-1}$, the surrounding loose crosslinking of the matrix, $I_{loose}(q) = k_{loose}(1 + q^2\xi_{loose}{}^2)^{-1}$, and the inter-microgel spacing within that matrix, $I_{micro}(q) = k_{micro}(1 + q^2\xi_{tight}{}^2)^{-1}\,F(q)$, further appended by the microgel form factor $F(q)$. [46], Copyright 2008.
Reproduced with permission from the American Chemical Society.

In a further variant of the preceding branch of studies, Papadakis, Patrickios, Gradzielski, and co-authors probed amphiphilic single- and double-network hydrogels by small-angle X-ray [138] and neutron scattering [139]. The SAXS data were fitted by a combined low-q Porod and a high-q Lorentzian term, along with a spherical core–shell form factor and a hard-sphere structure factor in the mid-q range to account for micellar aggregates of hydrophobic chain segments and crosslinkers coronated by hydrophilic chain segments and dangling chains within the networks.

Another popular material is the thermo- and environmentally sensitive poly(*N*-isopropylacrylamide) [135]. Just as with pEG-DA, the usual approach of hydrogel formation with this monomer is free-radical crosslinking polymerization conducted in the presence of a crosslinker, most typically *N*,*N*'-methylenebisacrylamide. An interplay of the uncontrolled course of this free-radical chain-growth process, complexed by different reactivities of these two monomers [140], along with an often insufficiently attenuated heat-up of the sample due to the enthalpy of polymerization [141,142] leads to a complex nanostructure that

displays several levels of inhomogeneity and heterogeneity. To consistently probe this structural complexity, Hashimoto and co-workers employed a conjoint set of Fourier-space light and neutron scattering along with real-space confocal laser scanning microscopy [46], as shown in Fig. 11. This investigation revealed that gels prepared at temperatures at and above 24.5 °C display a bi-continuous microphase-separated structure that consists of a gel phase interpenetrated by a solvent phase, as also shown in Fig. 11 (lower panel). The gel phase further consists of locally dense-crosslinked microgel clusters tied loosely together, as shown in Fig. 12. Fitting of the SANS data to a combined term of three Lorentzians denoting the microgel-internal tight crosslinking, $I_{\text{tight}}(q) = k_{\text{tight}}(1 + q^2\xi_{\text{tight}}{}^2)^{-1}$, the surrounding loose crosslinking of the matrix, $I_{\text{loose}}(q) = k_{\text{loose}}(1 + q^2\xi_{\text{loose}}{}^2)^{-1}$, and the inter-microgel spacing within that matrix, $I_{\text{micro}}(q) = k_{\text{micro}}(1 + q^2\xi_{\text{tight}}{}^2)^{-1}\ F(q)$, further appended by the microgel form factor $F(q)$, allowed this structure to be assessed quantitatively, as shown in Fig. 13. Moreover, additional USANS, SLS, and confocal laser scanning microscopy confirmed the quantification of the microgel size and spacing obtained from this fitting, and on top of that, served to further characterize the bi-continuous microphase-separated structure with a view to its inter-domain spacing and fractal dimension, as shown in Fig. 11.

5. Conclusions

Scattering methods based on spatial and temporal contrast fluctuations in a polymer-network gel, which originate from related polymer-segmental density fluctuations, reveal rich insight into nanostructurel inhomogeneity displayed by many of these valuable soft materials. The complementary contrasting provided by light, neutron, and X-ray scattering allows such information to be obtained on all length scales relevant in view of different levels of inhomogeneity encountered in polymeric gels. Furthermore, complementary use of both static and dynamic scattering methods allows the interplay and effect of these inhomogeneities to be unraveled. With that, scattering techniques provide an essential toolkit to assess the origin of formation of such nanostructural inhomogeneity in polymer-network gels; they also allow the modes of action that these inhomogeneities impart on the material properties to be substantiated. Both is a key to rationally designing polymer-network gels such to serve as advanced functional soft materials in their existing and prospective applications. Despite this promise, and despite the wide establishment of scattering techniques as standard analytical tools in polymer science, they should be employed with constant awareness about their physical principles. This awareness is particularly relevant in view of the risk of misinterpretation of scattering data that may be affected by various effects; as just one example, locally inhomogeneous hydrogen–deuterium exchange in SANS experiments shall be mentioned [143]. This review article targets to foster such conceptual understanding.

References

[1] Di Lorenzo F, Seiffert S. Nanostructural heterogeneity in polymer networks and gels. Polym Chem 2015;6:5515–28.
[2] Habicht A, Schmolke W, Lange F, Saalwächter K, Seiffert S. The non-effect of polymer network inhomogeneities in microgel volume phase transitions: support for the mean-field perspective. Macromol Chem Phys 2014;215:1116–33.
[3] Habicht A, Schmolke W, Goerigk G, Lange F, Saalwächter K, Ballauff M, et al. Critical fluctuations and static inhomogeneities in polymer gel volume phase transitions. J Polym Sci Part B 2015;53:1112–22.
[4] Modern Superabsorbent Polymer Technology.Buchholz FL, Graham AT, editors. New York: Wiley-VCH; 1997, 304 pp.
[5] Evans CH. Hydrogel Contact Lens. US 4,199,231 A; 1980.
[6] Nicolson PC, Vogt J. Soft contact lens polymers: an evolution. Biomaterials 2001;22:3273–83.
[7] Langer R, Peppas N. Chemical and physical structure of polymers as carriers for controlled release of bioactive agents: a review. J Macromol Sci C Polym Rev 1983;23:61–126.
[8] Hoarea TR, Kohane DS. Hydrogels in drug delivery: progress and challenges. Polymer 2008;49:1993–2007.
[9] Williams T. Gel permeation chromatography: a review. J Mater Sci 1970;5:811–20.
[10] Lambert A. Review of gel permeation chromatography. Br Polym J 1971;3:13–23.
[11] Dolnık V. DNA sequencing by capillary electrophoresis (review). J Biochem Biophys Methods 1999;41:103–19.
[12] Albarghouthi MN, Barron AE. Polymeric matrices for DNA sequencing by capillary electrophoresis. Electrophoresis 2000;21:4096–111.
[13] Zhu Z, Lu J, Liu S. Protein separation by capillary gel electrophoresis: a review. Anal Chim Acta 2012;709:21–31.
[14] Dušek K, Prins W. Structure and elasticity of non-crystalline polymer networks. Adv Polym Sci 1969;6:1–102.
[15] Matsuo ES, Orkisz M, Sun ST, Li Y, Tanaka T. Origin of structural inhomogeneities in polymer gels. Macromolecules 1994;27:6791–6.
[16] Norisuye T, Masui N, Kida Y, Ikuta D, Kokufuta E, Ito S, et al. Small angle neutron scattering studies on structural inhomogeneities in polymer gels: irradiation cross-linked gels vs chemically cross-linked gels. Polymer 2002;43:5289–97.
[17] Norisuye T, Kida Y, Masui N, Tran-Cong-Miyata Q, Maekawa Y, Yoshida M, et al. Studies on two types of built-in inhomogeneities for polymer gels: frozen segmental concentration fluctuations and spatial distribution of cross-links. Macromolecules 2003;36:6202–12.
[18] Moussaïd A, Slot HJM, Joosten JGH. Light scattering and gel inhomogeneities. Int J Polym Anal Charact 1995;2:43–53.
[19] Shibayama M, Takata S, Norisuye T. Static inhomogeneities and dynamic fluctuations of temperature sensitive polymer gels. Physica A 1998;249:245–52.
[20] Shibayama M. Spatial inhomogeneity and dynamic fluctuations of polymer gels. Macromol Chem Phys 1998;199:1–30.
[21] Koizumi S, Monkenbusch M, Richter D, Schwahn D, Farago B, Annaka M. Frozen concentration fluctuations in a poly(*N*-isopropyl acrylamide) gel studied by neutron spin echo and small-angle neutron scattering. Appl Phys A 2002;74:s399–401.
[22] Geissler E, Hecht AM, Horkay F. Nanoscale inhomogeneities and thermodynamics of unfilled polymer gels. J Macromol Sci B 2005;44:873–80.
[23] Horkay F, Basser PJ, Hecht AM, Geissler E. Structural investigations of a neutralized polyelectrolyte gel and an associating neutral hydrogel. Polymer 2005;46:4242–7.
[24] Bastide J, Leibler L. Large-scale heterogeneities in randomly cross-linked networks. Macromolecules 1988;21:2647–9.
[25] Rouf-George C, Munch JP, Schosseler F, Pouchelon A, Beinert G, Boué F, et al. Thermal and quenched fluctuations of polymer concentration in poly(dimethylsiloxane) gels. Macromolecules 1997;30:8344–59.
[26] Geissler E, Horkay F, Hecht AM, Rochas C, Lindner P, Bourgaux C, et al. Investigation of PDMS gels and solutions by small angle scattering. Polymer 1997;38:15–20. Erratum: Polymer 1997;38:2575.
[27] Panyukov S, Rabin Y. Statistical physics of polymer gels. Phys Rep 1996;269:1–131.
[28] Panyukov S, Rabin Y. Polymer gels: frozen inhomogeneities and density fluctuations. Macromolecules 1996;29:7960–75.
[29] Panyukov S, Potemkin I. Statics and dynamics of the liquid- and 'Solidlike' degrees of freedom in lightly cross-linked polymer networks. J Phys I 1997;7:273–89.
[30] Rabin Y, Panyukov S. Scattering profiles of charged gels: frozen inhomogeneities, thermal fluctuations, and microphase separation. Macromolecules 1997;30:301–12.
[31] Shibayama M, Norisuye T. Gel formation analyses by dynamic light scattering. Bull Chem Soc Jpn 2002;75:641–59.
[32] Ikkai F, Shibayama M. Inhomogeneity control in polymer gels. J Polym Sci Part B Polym Phys 2005;43:617–28.
[33] Asai M, Katashima T, Chung U.-i Sakai T, Shibayama M. Correlation between local and global inhomogeneities of chemical gels. Macromolecules 2013;46:9772–81.
[34] Grube S, Oppermann W. Inhomogeneity in hydrogels synthesized by Thiol–Ene polymerization. Macromolecules 2013;46:1948–55.
[35] Kizilay M, Okay O. Effect of hydrolysis on spatial inhomogeneity in poly(acrylamide) gels of various crosslink densities. Polymer 2003;44:5239–50.
[36] Kizilay MY, Okay O. Effect of initial monomer concentration on spatial inhomogeneity in poly(acrylamide) gels. Macromolecules 2003;36:6856–62.
[37] Orakdogen N, Kizilay MY, Okay O. Suppression of inhomogeneities in hydrogels formed by free-radical crosslinking copolymerization. Polymer 2005;46:11407–15.
[38] Orakdogen N, Okay O. Correlation between crosslinking efficiency and spatial inhomogeneity in poly(acrylamide) hydrogels. Polym Bull 2006;57:631–41.
[39] Orakdogen N, Okay O. Influence of the initiator system on the spatial inhomogeneity in acrylamide-based hydrogels. J Appl Polym Sci 2007;103:3228–37.

[40] Kuru EA, Orakdogen N, Okay O. Preparation of homogeneous polyacrylamide hydrogels by free-radical crosslinking copolymerization. Eur Polym J 2007;43:2913–21.
[41] Nishi K, Asai H, Fujii K, Han Y-S, Kim T-H, Sakai T, et al. Small-angle neutron scattering study on defect-controlled polymer networks. Macromolecules 2014;47:1801–9.
[42] Durmaz S, Okay O. Inhomogeneities in poly(acrylamide) gels: position-dependent elastic modulus measurements. Polym Bull 2001;46:409–18.
[43] Sayil C, Okay O. Macroporous poly(N-isopropyl)acrylamide networks: formation conditions. Polymer 2001;42:7639–52.
[44] Hecht AM, Duplessix R, Geissler E. Structural inhomogeneities in the range 2: 5–2500. ANG. in polyacrylamide gels. Macromolecules 1985;18:2167–73.
[45] Mallam S, Horkay F, Hecht AM, Geissler E. Scattering and swelling properties of inhomogeneous polyacrylamide gels. Macromolecules 1989;22:3356–61.
[46] Hirokawa Y, Okamoto T, Kimishima K, Jinnai H, Koizumi S, Aizawa K, et al. Sponge-like heterogeneous gels: hierarchical structures in poly(*N*-isopropylacrylamide) chemical gels as observed by combined scattering and confocal microscopy method. Macromolecules 2008;41:8210–9.
[47] Matsunaga T, Sakai T, Akagi Y, Chung UI, Shibayama M. SANS and SLS studies on tetra-arm PEG gels in as-prepared and swollen states. Macromolecules 2009;42:6245–52.
[48] Shibayama M. Small-angle neutron scattering on polymer gels: phase behavior, inhomogeneities and deformation mechanisms. Polym J 2011;43:18–34.
[49] Benoît H, Picot C. Étude par diffusion de la lumière des solutions macromoleculaires moyennement concentrées. Pure Appl Chem 1966;12:545–62.
[50] Koberstein JT, Picot C, Benoit H. Light and neutron scattering studies of excess low-angle scattering in moderately concentrated polystyrene solutions. Polymer 1985;26:673–81.
[51] Horkay F, Hecht AM, Geissler E. Small angle neutron scattering in poly(vinyl alcohol) hydrogels. Macromolecules 1994;27:1795–8.
[52] Benguigui L, Boué F. Homogeneous and inhomogenous polyacrylamide gels as observed by small angle neutron scattering: a connection with elastic properties. Eur Phys J B 1999;11:439–44.
[53] Horkay F, Burchard W, Hecht AM, Geissler E. Poly(vinyl alcohol-vinyl acetate) copolymer hydrogels: scattering and osmotic observations. Macromolecules 1993;26:3375–80.
[54] Hecht AM, Horkay F, Schleger P, Geissler E. Thermal fluctuations in polymer gels investigated by neutron spin echo and dynamic light scattering. Macromolecules 2002;35:8552–5.
[55] Shibayama M, Norisuye T, Nomura S. Cross-link density dependence of spatial inhomogeneities and dynamic fluctuations of poly(*N*-isopropylacrylamide) gels. Macromolecules 1996;29:8746–50.
[56] Koizumi S, Monkenbusch M, Richter D, Schwahn D, Farago B. Concentration fluctuations in polymer gel investigated by neutron scattering: static inhomogeneity in swollen gel. J Chem Phys 2004;121:12721–31.
[57] Shibayama M. Universality and specificity of polymer gels viewed by scattering methods. Bull Chem Soc Jpn 2006;79:1799–819.
[58] Shibayama M, Fujikawa Y, Nomura S. Dynamic light scattering study of poly(*N*-isopropylacrylamide-co-acrylic acid) gels. Macromolecules 1996;29:6535–40.
[59] Bastide J, Candau SJ. Structure of gels as investigated by means of static scattering. In: Cohen-Addad JP, editor. Physical Properties of Polymeric Gels. New York: John Wiley & Sons New York; 1996. p. 143–308.
[60] Norisuye T, Tran-Cong-Miyata Q, Shibayama M. Dynamic inhomogeneities in polymer gels investigated by dynamic light scattering. Macromolecules 2004;37:2944–53.
[61] Soni VK, Stein RS. Light scattering studies of poly(dimethylsiloxane) solutions and swollen networks. Macromolecules 1990;23:5257–65.
[62] Joosten JGH, McCarthy JL, Pusey PN. Dynamic and static light scattering by aqueous polyacrylamide gels. Macromolecules 1991;24:6690–9.
[63] Krahl F, Boyko V, Arndt KF. Characterization of spatial inhomogeneities and dynamic properties of random cross-linked polystyrene networks by dynamic light scattering. Polymer 2010;51:2576–84.
[64] Debye PP. A photoelectric instrument for light scattering measurements and a differential refractometer. J Appl Phys 1946;13:392–7.
[65] Debye P, Bueche AM. Scattering by an inhomogeneous solid. J Appl Phys 1949;20:518–25.
[66] Pekeris CL. Note on the scattering of radiation in an inhomogeneous medium. Phys Rev 1947;71:268.
[67] Cerid H, Okay O. Minimization of spatial inhomogeneity in polystyrene gels formed by free-radical mechanism. Eur Polym J 2004;40:579–87.
[68] Kizilay MY, Okay O. Effect of swelling on spatial inhomogeneity in poly(acrylamide) gels formed at various monomer concentrations. Polymer 2004;45:2567–76.
[69] Gundogan N, Okay O, Oppermann W. Elasticity swelling and spatial inhomogeneity of Poly(*N*, *N*-dimethylacrylamide) hydrogels formed at various polymer concentrations. Macromol Chem Phys 2004;205:814–23.
[70] Furukawa H, Horie K, Nozaki R, Okada M. Swelling-induced modulation of static and dynamic fluctuations in polyacrylamide gels observed by scanning microscopic light scattering. Phys Rev E 2003;68, 031406/1-14.
[71] Shibayama M, Shirotani Y, Shiwa Y. Static inhomogeneities and dynamics of swollen and reactor-batch polymer gels. J Chem Phys 2000;121:442–9.
[72] Nie J, Du B, Opperman W. Influence of formation conditions on spatial inhomogeneities in poly(*N*-isopropylacrylamide) hydrogels. Macromolecules 2004;37:6558–64.
[73] Abdurrahmanoglu S, Okay O. Homogeneous poly(acrylamide) hydrogels made by large size, flexible dimethacrylate cross-linkers. Macromolecules 2008;41:7759–61.
[74] Lindemann B, Schröder UP, Oppermann W. Influence of the cross-Linker reactivity on the formation of inhomogeneities in hydrogels. Macromolecules 1997;30:4073–7.
[75] Mallam S, Horkay F, Hecht AM, Rennie AR, Geissler E. Microscopic and macroscopic thermodynamic observations in swollen poly(dimethylsiloxane) networks. Macromolecules 1991;24:543–8.
[76] Shibayama M, Tanaka T, Han CC. Small angle neutron scattering study on poly(*N*-isopropyl acrylamide) gels near their volume-phase transition temperature. J Chem Phys 1992;97:6829–41.
[77] Ornstein LS, Zernike F. Accidental deviations of density and opalescence at the critical point of a single substance. Proc Akad Sci 1914;17:793–806.
[78] Shibayama M, Ikkai F, Shiwa Y, Rabin Y. Effect of degree of cross-linking on spatial inhomogeneity in charged gels: I. Theoretical predictions and light scattering study. J Chem Phys 1997;107:5227–35.
[79] Ikkai F, Shibayama M, Han CC. Effect of degree of cross-linking on spatial inhomogeneity in charged gels: 2. small-angle neutron scattering study. Macromolecules 1998;31:3275–81.
[80] Shibayama M, Kawakubo K, Norisuye T. Comparison of the experimental and theoretical structure factors of temperature sensitive polymer gels. Macromolecules 1998;31:1608–14.
[81] Ikkai F, Shibayama M. Anomalous cross-link density dependence of scattering from charged gels. Phys Rev E 1997;56:R51–4.
[82] Takata S.-i Norisuye T, Shibayama M. Small-Angle neutron-Scattering study on preparation temperature dependence of thermosensitive gels. Macromolecules 2002;35:4779–84.
[83] Pusey PN, Van Megen W. Dynamic light scattering by non-ergodic media. Physica A 1989;157:705–41.
[84] Siegert AJF. On the fluctuations in signals returned by many independently moving scatterers MIT Radiat. Lab Rep. No. 465. Cambridge, Massachusetts Institute of Technology; 1943. p. 28.
[85] Takata SI, Norisuye T, Shibayama M. Preparation temperature dependence and effects of hydrolysis on static inhomogeneities of poly(acrylamide) gels. Macromolecules 1999;32:3989–93.
[86] Wun KL, Carlson FD. Harmonically bound particle model for quasi-elastic light scattering by gels. Macromolecules 1975;8:190–4.
[87] Rodd AB, Dunstan DE, Boger DV, Schmidt J, Burchard W. Heterodyne and nonergodic approach to dynamic light scattering of polymer gels: aqueous xanthan in the presence of metal ions (Aluminum(III)). Macromolecules 2001;34:3339–52.
[88] Joosten JGH, Geladé ETF, Pusey PN. Dynamic light scattering by nonergodic media: brownian particles trapped in polyacrylamide gels. Phys Rev A 1990;42:2161–75.
[89] Tanaka T, Hocker LO, Benedek GB. Spectrum of light scattered from a viscoelastic gel. J Chem Phys 1973;59:5151–9.
[90] De Gennes PG. Scaling Concepts in Polymer Physics. Ithaca, London: Cornell University Press; 1979, 324 pp.
[91] Hecht AM, Guillermo A, Horkay F, Mallam S, Legrand JF, Geissler E. Structure and dynamics of a poly(dimethylsiloxane) network: a comparative investigation of gel and solution. Macromolecules 1992;25:3677–84.
[92] Mendes Jr E, Lindner P, Buzier M, Boué F, Bastide J. Experimental evidence for inhomogeneous swelling and deformation in statistical gels. Phys Rev Lett 1991;66:1595–8.
[93] Liu R, Oppermann W. Spatial inhomogeneities of polystrene gels prepared from semidilute solutions. Macromolecules 2006;39:4159–67.
[94] Hiroi T, Ohl M, Sakai T, Shibayama M. Multiscale dynamics of inhomogeneity-free polymer gels. Macromolecules 2014;47:763–70.
[95] Moussaïd A, Pusey PN, Slot JM, Joosten JGH. Simulation of scattering properties of gels. Macromolecules 1999;32:3774–87.
[96] Furukawa H, Hirotsu S. Dynamic light scattering from static and dynamic fluctuations in inhomogeneous media. J Phys Soc Jpn 2002;71:2873–80.
[97] Xue JZ, Pine DJ, Milner ST, Wu XI, Chaikin PM. Nonergodicity and light scattering from polymer gels. Phys Rev A 1992;46:6550–63.
[98] Manno M, Bulone D, Martorana V, San Biagio PL. Ergodic to non-ergodic transition monitored by scattered light intensity statistics. Physica A 2004;341:40–54.
[99] Fang L, Brown W. Dynamic light scattering by permanent gels: heterodyne and nonergodic medium methods of data evaluation. Macromolecules 1992;25:6897–903.
[100] Frisken BJ. Revisiting the method of cumulants for the analysis of dynamic light-scattering data. Appl Optics 2001;40:4087–91.
[101] Blanco MC, Leisner D, Vázquez C, López-Quintela MA. Dynamic light scattering in transient reversible gels. Langmuir 2000;16:8585–94.
[102] Michel E, Cipelletti L, d'Humieres E, Gambin Y, Urbach W, Porte G, et al. Self-diffusion and collective diffusion in a model viscoelastic system. Phys Rev E 2002;66, 031402/1-7.
[103] Dai S, Tam KC, Jenkins RD. Dynamic light scattering of semi-dilute hydrophobically modified alkali-soluble emulsion solutions with varying length of hydrophobic alkyl chains. Macromol Chem Phys 2002;203:2312–21.

[104] Narita T, Mayumi K, Ducouret G, Hébraud P. Viscoelastic properties of poly(vinyl alcohol) hydrogels having permanent and transient cross-links studied by microrheology, classical rheometry, and dynamic light scattering. Macromolecules 2013;46:4174–83.
[105] Dogu S, Oppermann W. Influence of observation temperature on light scattering of poly-N-isopropylacrylamide hydrogels. Soft Matter 2012;8:2705–13.
[106] Geissler E, Horkay F, Hecht AM. Scattering from network polydispersity in polymer gels. Phys Rev Lett 1993;71:645–8.
[107] Ngai T, Wu C, Chen Y. Origins of the speckles and slow dynamics of polymer gels. J Phys Chem B 2004;108:5532–40.
[108] Yang Z, Hemar Y, Hilliou L, Gilbert EP, McGillivray DJ, Williams MAK, et al. Nonlinear behavior of gelatin networks reveals a hierarchical structure. Biomacromolecules 2016;17:590–600.
[109] Mallam S, Hecht AM, Geissler E, Pruvost P. Structure of swollen polydimethyl siloxane gels. J Chem Phys 1989;91:6447–54.
[110] Horkay F, Hecht AM, Grillo I, Basser PJ, Geissler E. Experimental evidence for two thermodynamic length scales in neutralized polyacrylate gels. J Chem Phys 2002;117:9103–6.
[111] Tokita M, Tanaka T. Friction coefficient of polymer networks of gels. J Chem Phys 1991;65:4613–9.
[112] Horkay F, Hecht AM, Geissler E. Fine structure of polymer networks as revealed by solvent swelling. Macromolecules 1998;31:8851–6.
[113] Cohen Y, Ramon O, Kopelman IJ, Mizrahi S. Characterization of inhomogeneous polyacrylamide gels. J Polym Sci Part B Polym Phys 1992;30:1055–67.
[114] Rouf C, Bastide J, Pujol JM, Schosseler F, Munch JP. Strain effect on quasistatic fluctuations in a polymer gel. Phys Rev Lett 1994;73:830–3.
[115] Mendes E, Girard B, Picot C, Buzier M, Boué F, Bastide J. Small-angle neutron scattering study of end-linked gels. Macromolecules 1993;26:6873–7.
[116] Mendes E, Oeser R, Hayes C, Boué F, Bastide J. Small-angle neutron scattering study of swollen elongated gels: butterfly patterns. Macromolecules 1996;29:5574–84.
[117] Bastide J, Leibler L, Prost J. Scattering by deformed swollen gels: butterfly isointensity patterns. Macromolecules 1990;23:1821–5.
[118] Onuki A. Scattering from deformed swollen gels with heterogeneities. J Phys II 1992;2:45–61.
[119] Zhao Y, Zhang G, Wu C. Nonergodic dynamics of a novel thermally sensitive hybrid gel. Macromolecules 2001;34:7804–8.
[120] Travas-Sejdic J, Easteal A, Knott R, Pedersen JS. Small-angle neutron scattering from poly(NIPA-co-AMPS) gels. J Appl Cryst 2000;33:735–9.
[121] Ikkai F, Suzuki T, Karino T, Shibayama M. Microstructure of *N*-isopropylacrylamide-Acrylic acid copolymer gels having different spatial configurations of weakly charged groups. Macromolecules 2007;40:1140–6.
[122] Hild G. Model networks based on 'endlinking' processes: synthesis, structure and properties. Prog Polym Sci 1998;23:1019–149.
[123] Urayama K, Kawamura T, Hirata Y, Kohjiya S. SAXS study on poly(dimethylsiloxane) networks with controlled distributions of chain lengths between crosslinks. Polymer 1998;39:3827–33.
[124] Sakai T, Matsunaga T, Yamamoto Y, Ito C, Yoshida R, Suzuki S, et al. Design and fabrication of a high-strength hydrogel with ideally homogeneous network structure from tetrahedron-like macromonomers. Macromolecules 2008;41:5379–84.
[125] Matsunaga T, Sakai T, Akagi Y, Chung UI, Shibayama M. Structure characterization of tetra-PEG gel by small-angle neutron scattering. Macromolecules 2009;42:1344–51.
[126] Oeser R, Ewen B, Richter D, Farago B. Dynamic fluctuations of crosslinks in a rubber: a neutron-spin-echo study. Phys Rev Lett 1988;60:1041–4.
[127] Sakar A, Gosh K. Molecular association in polyethylene glycol. Kolloid Z Z Polym 1970;236:140–2.
[128] Zander ZK, Hua G, Wiener CG, Vogt BD, Becker ML. Control of mesh size and modulus by kinetically dependent cross-linking in hydrogels. Adv Mater 2015;27:6283–8.
[129] Saffer EM, Lackey MA, Griffin DM, Kishore S, Tew GN, Bhatia SR. SANS study of highly resilient poly(ethylene glycol) hydrogels. Soft Matter 2014;10:1905–16.
[130] Kurakazu M, Katashima T, Chijiishi M, Nishi K, Akagi Y, Matsunaga T, et al. Evaluation of gelation kinetics of tetra-PEG gel. Macromolecules 2010;43:3935–40.
[131] Matsunaga T, Asai H, Akagi Y, Sakai T, Chung UI, Shibayama M. SANS studies on tetra-PEG gel under uniaxial deformation. Macromolecules 2011;44:1203–10.
[132] Akagi Y, Katashima T, Katsumoto Y, Fujii K, Matsunaga T, Chung UI, et al. Examination of the theories of rubber elasticity using an ideal polymer network. Macromolecules 2011;44:5817–21.
[133] Akagi Y, Gong JP, Chung UI, Sakai T. Transition between phantom and affine network model observed in polymer gels with controlled network structure. Macromolecules 2013;46:1035–40.
[134] Shibayama M. Structure-mechanical property relationship of tough hydrogels. Soft Matter 2012;8:8030–8.
[135] Schild HG. Poly(N-isopropylacrylamide): experiment, theory and application. Prog Polym Sci 1992;17:163–249.
[136] Malo de Molina P, Lad S, Helgeson ME. Heterogeneity and its influence on the properties of difunctional poly(ethylene glycol) hydrogels: structure and mechanics. Macromolecules 2015;48:5402–11.
[137] Ajith C, Deshpande AP, Varughese S. Proton conductivity in crosslinked hydrophilic ionic polymer system: competitive hydration, crosslink heterogeneity, and ineffective domains. J Polym Sci PartB Polym Phys 2016;54:1087–101.
[138] Zhang X, Kyriakos K, Rikkou-Kalourkoti M, Kitiri EN, Patrickios CS, Papadakis CM. Amphiphilic single and double networks: a small-angle X-ray scattering investigation. Colloid Polym Sci 2016;294:1027–36.
[139] Vamvakaki M, Patrickios CS, Lindner P, Gradzielski M. Amphiphilic networks based on cross-linked star polymers: a small-angle neutron scattering study. Langmuir 2007;23:10433–7.
[140] Wu X, Pelton RH, Hamielec AE, Woods DR, McPhee W. The kinetics of poly(N-isopropylacrylamide) microgel latex formation. Colloid Polym Sci 1994;272:467–77.
[141] Gehrke SH, Palasis M, Akhtar K. Effect of synthesis conditions on properties of poly(N-isopropylacrylamide) gels. Polym Int 1992;29:29–36.
[142] Kara S, Okay O, Pekcan O. Real-time temperature and photon transmission measurements for monitoring phase separation during the formation of poly(N-isopropylacrylamide) gels. J Appl Polym Sci 2002;86:3589–95.
[143] Banc A, Charbonneau C, Dahesh M, Appavou MS, Fu Z, Morel MH, et al. Small angle neutron scattering contrast variation reveals heterogeneities of interactions in protein gels. Soft Matter 2016;12:5340–52.